Published in final edited form as:

Pain. 2016 July ; 157(7): 1448–1463. doi:10.1097/j.pain.0000000000000555.

(*S*)-Lacosamide inhibition of CRMP2 phosphorylation reduces postoperative and neuropathic pain behaviors through distinct classes of sensory neurons identified by constellation pharmacology

Aubin Moutal[a,1], **Lindsey A. Chew**[a,1], **Xiaofang Yang**[a], **Yue Wang**[a], **Seul Ki Yeon**[b], **Edwin Telemi**[a], **Seeneen Meroueh**[c], **Ki Duk Park**[b], **Raghuraman Shrinivasan**[d], **Kerry B. Gilbraith**[a], **Chaoling Qu**[a], **Jennifer Y. Xie**[a], **Amol Patwardhan**[a], **Todd W. Vanderah**[a], **May Khanna**[a], **Frank Porreca**[a], and **Rajesh Khanna**[a,*]

[a]Department of Pharmacology, College of Medicine, University of Arizona, Tucson, AZ 85742, USA

[b]Department of Biological Chemistry, University of Science and Technology and Center for Neuro-Medicine, Brain Science Institute, Korea Institute of Science and Technology, Seoul 136-791, Republic of Korea

[c]Wayne State University, Detroit, MI, 48202

[d]Department of Biology, University of Utah, Salt Lake City, UT 84112, USA

Keywords

CaV2.2; CRMP2; (*S*)-lacosamide; constellation pharmacology; calcium imaging; post-operative pain; neuropathic pain

INTRODUCTION

The N-type voltage-gated calcium channel (CaV2.2) is a control point for synaptic activity in nociceptive circuits [84]. The potential of targeting this point of convergence has been demonstrated by data showing the effect of selective conotoxins on allodynia [55] and the altered pain behavioral phenotype of transgenic mice lacking α_{1B}, the pore forming subunit of CaV2.2 [36; 37]. Furthermore, the CaV2.2-selective blocker Ziconotide (Prialt®) [44] and the α2δ subunit-targeted antiepileptic drug gabapentin (GBP; Neurontin®) are clinically effective and have been developed to target different components of the CaV2.2 channel complex [1; 27; 72]. Both drugs, however, are encumbered with problematic side effects as well as difficult dosing regimens [53; 54; 57; 67]. The development of novel CaV2.2-targeted drugs with improved efficacy and therapeutic index is highly desirable [50].

*To whom correspondence should be addressed: Dr. Rajesh Khanna, Department of Pharmacology, College of Medicine, University of Arizona, 1501 North Campbell Drive, P.O. Box 245050, Tucson, AZ 85724, USA Office phone: (520) 626-4281; Fax: (520) 626-2204; rkhanna@email.arizona.edu.

[1]co-first authors

Conflict of interest – There is no conflict of interest for any of the authors.

Inhibitory control of CaV2.2 activity by opioid receptor coupled GPCRs has been long established to reduce neuronal excitability and dampen nociceptive signaling in animal pain models (for a review, see [20]). We have recently advanced an innovative strategy targeting protein interactions modulating CaV2.2 as an alternative to direct channel block [8; 24; 29; 76; 79]. Targeting *channel regulation* may potentially lessen many of the adverse side effects associated with *direct* channel block. Supporting this concept, we reported that targeting CaV2.2 *indirectly* with a peptide derived from the collapsin response mediator protein 2 (CRMP2) peptide did not affect memory retrieval, motor coordination, depression-associated behaviors [8] and was not rewarding/addictive [29].

In the search of small molecules that may mimic the indirect regulation bestowed by the CRMP2 peptide, we identified (*S*)-Lacosamide ((*S*)-LCM), an enantiomer of the clinically approved anti-epileptic drug (*R*)-N-benzyl 2-acetamido-3-methoxypropionamide ((*R*)-LCM) or Vimpat®. Vimpat is used clinically for adjunctive control of epileptic seizures [5] and has also been approved for treatment of painful diabetic neuropathy [52]. Vimpat modulates slow inactivation of Na^+ channels [22; 56] with an IC_{50} of 80 μM [71]. Critically, we and others have demonstrated that at doses active *in vivo* for inhibition of seizures, (*R*)-LCM does not modulate Ca^{2+} activity [70].

In contrast to (*R*)-LCM, we recently reported that (*S*)-LCM has preferential activity on Ca^{2+} channels through the inhibition of CRMP2 phosphorylation by cyclin dependent kinase 5 (Cdk5) [47]. In line with this finding, we reported that Cdk5-mediated phosphorylation of CRMP2 strengthens its interactions with CaV2.2 both biochemically and functionally [10]. This outcome provides a rationale for the testing of (*S*)-LCM in painful conditions. Here, we asked if (*S*)-LCM inhibits Ca^{2+} influx in sensory neurons and produces antinociceptive effects by curtailing Cdk5-mediated phosphorylation of CRMP2. Additionally, we used constellation pharmacology, a paradigm for functional fingerprinting of neurons [64], to identify classes of neurons targeted by (*S*)-LCM.

METHODS

Animals

Pathogen-free, adult male Sprague–Dawley rats (150–200 g; Harlan Laboratories) were housed in temperature (23±3 °C) and light (12-h light/12-h dark cycle; lights on 07:00–19:00) controlled rooms with standard rodent chow and water available ad libitum. All experiments were approved by the Institutional Animal Care and Use Committee of the College of Medicine at the University of Arizona. All procedures were conducted in accordance with the Guide for Care and Use of Laboratory Animals published by the National Institutes of Health and the ethical guidelines of the International Association for the Study of Pain. Animals were randomly assigned to treatment or control groups for the behavioral experiments. All behavioral experiments were performed by an experimenter blinded to treatments.

Primary dorsal root ganglion (DRG) neuronal cultures

Sensory DRG neurons from Sprague-Dawley rats were isolated as described previously [8; 21]. Dorsal root ganglia (from thoracic 2 to lumbar 6 spinal levels) were excised aseptically and placed in Hank buffered salt solution (HBSS, Life technologies) containing penicillin (100 U/mL) and streptomycin (100 μg/mL, Cat# 15140, Life technologies) on ice. The ganglia were dissociated enzymatically by a 45 min incubation (37°C) in a DMEM (Cat# 11965, Life technologies) solution containing neutral protease (3.125 $mg.ml^{-1}$, Cat#LS02104, Worthington) and collagenase Type I (5 $mg.ml^{-1}$, Cat# LS004194, Worthington). The dissociated cells were resuspended in complete DRG medium, DMEM containing penicillin (100 U/mL), streptomycin (100 μg/mL), 30 $ng.ml^{-1}$ nerve growth factor and 10% fetal bovine serum (Hyclone). For Ca^{2+} imaging, the cells were seeded on poly-D-lysine (Cat# P6407, Sigma) coated glass coverslips (Cat# 72196-15, electron microscopy sciences) as a drop of 20 μl on the center of each coverslip, then placed in a 37°C, 5 % CO_2 incubator for 45–60 min to allow cells to attach. Then the cultures were flooded by gently adding complete DRG medium on the edge of each well to avoid detaching any weakly adherent cell. For immunoblotting, dissociated DRG neurons from 1 rat, were plated in a poly-D-lysine coated 12 well plate and placed in a 37°C, 5 % CO_2 incubator. All cells were used within 24 hours after seeding

Western blotting

For examining the effect of (*R*)- or (*S*)-LCM on CRMP2 phosphorylation state, DRGs were treated for 30 min with the drugs and then lysed using RIPA buffer (50mM Tris-HCl, pH 7.4, 50mM NaCl, 2mM $MgCl_2$, 1% [vol/vol] NP40, 0.5% [mass/vol] sodium deoxycholate, and 0.1% [mass/vol] sodium dodecyl sulfate). Protease (Cat# B14002; Biotool) and phosphatase inhibitors (Cat# B15002, Biotool), and BitNuclease (Cat# B16002, Biotool) were included in RIPA buffer. Protein concentrations were determined using the BCA protein assay (Cat# PI23225, Thermo Fisher Scientific). Approximately 3μg of total proteins were loaded on an SDS-PAGE and then transferred to polyvinylidene difluoride membranes and blocked at room temperature for 1 hour in TBST (50 mM Tris-HCl, pH 7.4, 150 mM NaCl, 0.1 % Tween 20), 5% non-fat dry milk. Primary antibodies used for probing were CRMP2 (Cat# C2993, Sigma), CRMP2 pSer522 (Cat# CP2191, ECM Biosciences), and βIII-tubulin (Cat# G712A, Promega,) diluted in TBST with 5% bovine serum albumin. Immunoblots were revealed by enhanced luminescence (WBKLS0500, Millipore) before exposure to a photographic film. Films were scanned, digitized, and quantified using Un-Scan-It gel version 6.1 scanning software (Silk Scientific Inc).

Calcium imaging

DRG neurons were loaded at 37°C with 3μM Fura-2AM (Cat#F-1221, Life technologies, stock solution prepared at 1mM in DMSO, 0.02% pluronic acid, Cat#P-3000MP, Life technologies) for 30 minutes (K_d= 25μM, λ_{ex} 340, 380 nm/λ_{emi} 512 nm) to follow changes in intracellular calcium ($[Ca^{2+}]_c$) in Tyrode's solution (at ~310 mOsm) containing 119 mM NaCl, 2.5mM KCl, 2mM $MgCl_2$, 2mM $CaCl_2$, 25mM HEPES, pH 7.4 and 30mM glucose. The solution was supplemented with 500nM tetrodotoxin (TTX, voltage-gated Na^+ channel inhibitor) and 1 μM nifedipine (L-type voltage-gated Ca^{2+} channel inhibitor). Incubation

with either (*R*)-LCM (200 μM) or (*S*)-LCM (200 μM, 20 μM, 2 μM, 200 nM, 20 nM, or 2 nM) was done during the loading of the cells with Fura-2AM and the drugs were also added to the excitatory solution. All calcium-imaging experiments were done at room temperature (~23°C), except those involving bath applications of innocuous (17°C) or cold (4°C) temperature stimuli. To isolate the contributions of particular channel subtypes, we used the following subunit-selective blockers (all purchased from Alomone Labs, Jerusalem): Nifedipine (10 μM, L-type); ω-agatoxin GIVA (200 nM, P/Q-type) [45]; ω-conotoxin-GVIA (500 nM, N-type) [25]; SNX-482 (200 nM, R-type) [48]; and 3,5-dichloro-N-[1–(2,2-dimethyl-tetrahydro-pyran-4-ylmethyl)-4-fluoro-piperidin-4-ylmethyl]-benzamide (TTA-P2, 1 μM, T-type) [14]. Baseline was acquired for 1 minute followed by stimulation (15 sec) with an excitatory solution (at ~310 mOsm) comprised of 32mM NaCl, 90mM KCl, 2mM $MgCl_2$, 2mM $CaCl_2$, 25mM HEPES, pH 7.4 and 30mM glucose. Fluorescence imaging was performed with an inverted microscope, Nikon Eclipse T*i*-U (Nikon Instruments Inc.), using objective Nikon Super Fluor MTB FLUOR 10× 0.50 and a Photometrics cooled CCD camera CoolSNAP ES^2 (Roper Scientific) controlled by NIS Elements software (version 4.20, Nikon instruments). The excitation light was delivered by a Lambda-LS system (Sutter Instruments). The excitation filters (340±5 nm and 380±7 nm) were controlled by a Lambda 10-2 optical filter change (Sutter Instruments). Fluorescence was recorded through a 505 nm dichroic mirror at 535±25 nm. To minimize photobleaching and phototoxicity, the images were taken every 10 seconds during the time-course of the experiment using the minimal exposure time that provided acceptable image quality. The changes in $[Ca^{2+}]_c$ were monitored by following the ratio of F_{340}/F_{380}, calculated after subtracting the background from both channels.

Whole-cell voltage-clamp electrophysiology

Recordings were obtained from acutely dissociated DRG neurons as described. To isolate calcium currents, Na^+ and K^+ currents were blocked with 500 nM tetrodotoxin (TTX; Alomone Laboratories) and 30 mM tetraethylammonium chloride (TEA-Cl; Sigma). Extracellular recording solution (at ~310 mOsm) consisted of the following (in mM): 110 *N*-methyl-D-glucamine (NMDG), 10 $BaCl_2$, 30 TEA-Cl, 10 HEPES, 10 glucose, pH at 7.4, 0.001 TTX, 0.01 nifedipine. The intracellular recording solution (at ~310 mOsm) consisted of the following (in mM): contained 150 CsCl2, 10 HEPES, 5 Mg-ATP, 5 BAPTA, pH at 7.4. Fire-polished recording pipettes, 2 to 5 MV resistances were used for all recordings. Whole-cell recordings were obtained with a HEKA EPC-10 USB (HEKA Instruments Inc.); data were acquired with a Patchmaster (HEKA) and analyzed with a Fitmaster (HEKA). Capacitive artifacts were fully compensated, and series resistance was compensated by ~70%. Recordings made from cells with greater than a 5 mV shift in series resistance compensation error were excluded from analysis. All experiments were performed at room temperature (~23°C).

Constellation pharmacology

These experiments were performed as described previously [64], but with the following modifications. DRG neurons were loaded at 37°C with 3μM Fura-2AM for 30 minutes in Tyrode's solution. After a 1 minute baseline measurement Ca^{2+} influx was stimulated by the addition of the following receptor agonists: 400 nM menthol, 50 μM histamine, 10 μM

adenosine triphosphate (ATP), 200 μM allyl isothiocyanate (AITC), 1 mM acetylcholine (Ach), 100 nM capsaicin diluted in Tyrode's solution (without TTX or Nifedipine). At the end of the constellation pharmacology protocol, cell viability was assessed by depolarization-induced Ca^{2+} influx using and an excitatory KCl solution comprised of 32mM NaCl, 90mM KCl, 2mM $MgCl_2$, 2mM $CaCl_2$, 25mM HEPES, pH 7.4, 30mM glucose. After the 1-minute baseline measurement, each trigger was applied for 15-seconds in the order indicated above in 6-minute intervals. Following each trigger, bath solution was continuously perfused over the cells to wash off excess of the trigger. This process was automated using the software WinTask ×64 (Version 5.1, WinTask) that controlled the perfusion of the standard bath solution and triggers through Valvelink 8.2 software (Automate Scientific). For the (*S*)-LCM condition, 10 μM (*S*)-LCM was added to the Tyrode's solution during the loading with Fura-2AM, as well as to each of the solutions containing a trigger. Fluorescence imaging was performed under the same conditions noted above for calcium imaging. A cell was defined as a 'responder' if its fluorescence ratio of 340nm/380nm was greater than 10% of the baseline value calculated using the average fluorescence in the 30 seconds preceding application of the trigger.

Indwelling intrathecal catheter

Rats were anesthetized (ketamine/xylazine anesthesia, 80/12 mg/kg i.p., Sigma) and placed in a stereotaxic head holder. The cisterna magna was exposed and incised, and an 8 cm catheter (PE-10, Stoelting) was implanted as previously reported, terminating in the lumbar region of the spinal cord [80]. Catheters were sutured (3-0 silk suture) into the deep muscle and externalized at the back of the neck; skin was closed with autoclips and hindpaw incision or spared nerve injury was performed after a 5–7 day recovery period.

Paw incision model of postoperative pain

An animal model of surgical pain was generated by plantar incision as previously described [7]. Male Sprague-Dawley rats were anesthetized with isoflurane vaporized through a nose cone. The plantar aspect of the left hind paw was scrubbed with betadine and 70% alcohol 3 times. A 1 cm long incision, starting 0.5 cm from the heel and extending toward the toes, was made with a number 11 blade, through the skin and fascia of the plantar aspect of the left hind paw including the underlying muscle. The plantaris muscle was then elevated and longitudinally incised, leaving the muscle origin and insertion intact. After hemostasis with gentle pressure, the skin was closed with 2 mattress sutures of 5-0 nylon on a curved needle. Rats received an injection of gentamicin (1 mL/kg of 8 mg/mL solution, s.c.) and were allowed to recover from the anesthesia before returning to their home cage. Sham animals were anesthetized and the left hind paw scrubbed with betadine 3 times, then 70% ethanol, but no incision was made. Animals were allowed to recover for 24 hours, and then paw withdrawal thresholds were measured at 24 hours after surgery.

Spared Nerve Injury (SNI)

Under isoflurane anesthesia (5 % induction, 2.5 % maintenance in 2L/min air), skin on the lateral surface of the left hind thigh was incised. The biceps femoris muscle was bluntly dissected to expose the three terminal branches of the sciatic nerve [18]. Briefly, the common peroneal and tibial branches were tightly ligated with 4-0 silk and axotomized 2.0

mm distal to the ligation. Sham animals underwent the same operation; however the nerves were exposed and not ligated. Closure of the incision was made in two layers. The muscle was sutured once with 5-0 absorbable suture and skin was auto-clipped. Animals were allowed to recover for 5–7 days before any testing.

Spinal nerve ligation (SNL)

Nerve ligation injury produces signs of neuropathic dysesthesias, including tactile allodynia and thermal hypersensitivity. All nerve operations occurred 5 days after intrathecal catheter implantation. Rats were anesthetized with 2% isoflurane in O_2 anesthesia delivered at 2 L/min. The skin over the caudal lumbar region was incised and the muscles retracted. The L_5 and L_6 spinal nerves were exposed, carefully isolated, and tightly ligated with 4-0 silk distal to the dorsal root ganglion without limiting the use of the left hind paw of the animal. All animals were allowed 7 days to recover before any behavioral testing. Any animals exhibiting signs of motor deficiency were euthanized.

Data analysis

The statistical significance of differences between means was determined by either parametric or non-parametric analysis of variance (ANOVA) followed by post hoc comparisons (Dunnett or Tukey test) using GraphPad Software. Constellation pharmacology data was analyzed using Sigma Plot 12.5 and compared by z-test. All behavioral data was analyzed by non-parametric two-way analysis of variance (ANOVA; *post hoc*: Student-Neuman–Kuels) in FlashCalc (Dr. Michael H. Ossipov, University of Arizona, Tucson, AZ, USA); areas under the curve were compared by one-way ANOVA. Differences were considered to be significant if $p \leq 0.05$. All data were plotted in GraphPad Prism 6.

RESULTS

(S)-lacosamide inhibits CRMP2 phosphorylation in sensory neurons

We previously reported that (*S*)-LCM binds to CRMP2 [78] and inhibits its phosphorylation by Cdk5 in cortical neurons [47]. Here, we asked if a similar mechanism exists in sensory neurons. DRG neurons were incubated for 30 min with 2 or 200μM concentrations of (*S*)-LCM or 200μM of (*R*)-LCM treatment; CRMP2 binds to these enantiomers with an almost similar affinity – Kd of 1μM for (*R*)-LCM versus 1.5μM for (*S*)-LCM [77; 78]. Immunoblot analyses of lysates prepared from DRGs exposed thusly did not change the expression of total CRMP2 between the conditions (Fig. 1A, B). While 200 μM (*R*)-LCM had no effect on CRMP2 phosphorylation, the same concentration of (*S*)-LCM inhibited CRMP2 phosphorylation by Cdk5 by ~29% compared to control (Fig. 1A, C). At a concentration (i.e. 2 μM) approximating its binding affinity for CRMP2, (*S*)-LCM still effectively blocked Cdk5-mediated CRMP2 phosphorylation by ~29% compared to control (Fig. 1A, C). These results demonstrate a selective and potent inhibition of CRMP2 phosphorylation by (*S*)-LCM.

(S)-lacosamide inhibits K^+-evoked Ca^{2+} influx in sensory neurons

CRMP2 phosphorylation by Cdk5 strengthens the CRMP2-CaV2.2 thereby sensitizing Ca^{2+} influx [7]. Inhibiting this interaction and CRMP2 phosphorylation by (*S*)-LCM inhibits Ca^{2+}

influx via CaV2.2 in cortical neurons [47]. Thus, we asked if (*S*)-LCM could inhibit K^+-evoked Ca^{2+} influx in sensory neurons following a 30-min incubation, a time at which when CRMP2 phosphorylation is inhibited. Calcium imaging experiments performed with Fura-2AM on rat DRG neurons demonstrated that stimulation with high 90 mM KCl (a concentration where mostly CaV2 channels are recruited [75]) produced a transient rise in intracellular calcium ($[Ca^{2+}]_c$). Peak calcium influx was recorded within 20 sec of stimulation (Fig. 2A). In DRGs incubated for 30 min with 200μM (*S*)-LCM, K^+-evoked Ca^{2+} response was decreased by ~88% compared to control (i.e. vehicle) treatment (Fig. 2B). Concurrent inhibition with 200μM (*S*)-LCM and a Cdk5 inhibitor (AT7519, 100 nM) or a CRMP2/CaV2.2 blocking peptide (myr-tat-CBD3, 10 μM [28]) did not produce any additional inhibition of K^+-evoked Ca^{2+} responses (Supplementary Fig. 1A). In contrast, (*R*)-LCM had the opposite effect, significantly increasing the K^+-evoked Ca^{2+} response of sensory neurons by ~136% (Fig. 2B). A concentration-response analysis indicated that (*S*)-LCM inhibited Ca^{2+} influx in a concentration dependent manner with an IC_{50} value of ~1.3 ± 0.3 μM (Fig. 2C). This value is in agreement with an IC_{50} value of ~2.8 μM for inhibition of Ca^{2+} influx for a membrane-tethered CRMP2 peptide that uncouples the CRMP2-CaV2.2 interaction that we recently reported [29]. Moreover, this value is better than TROX-1, a small-molecule, state-dependent blocker of CaV2 channels, which reduced the Ca^{2+} transient with an estimated IC_{50} value of 2.1 μM [1]. To confirm that (*S*)-LCM-mediated decreased in K^+-evoked Ca^{2+} was via CaV2.2, we used two different approaches. First, an additional pre-treatment using the selective CaV2.2 blocker, ω-conotoxin GVIA, did not produce any additional inhibition of K^+-evoked Ca^{2+} response (Supplementary Fig. 1B), suggesting that CaV2.2 is the major Ca^{2+} channel targeted by (*S*)-LCM. Second, we pharmacologically isolated each Ca^{2+} channel subtype to assess the effects of (*S*)-LCM on each subtype. (*S*)-LCM did not inhibit Ca^{2+} influx via L-, P/Q-, R- and T-type channels (Fig. 2D). (*S*)-LCM inhibited Ca^{2+} influx via N-type channels by ~74% (Fig. 2D). Thus, the small molecule (*S*)-LCM–mediated inhibition of CRMP2 phosphorylation by Cdk5 to curb Ca^{2+} influx represents a novel strategy for the modulation of CaV2.2 activity.

(S)-lacosamide decreases Ca^{2+} currents in sensory neurons

We have previously shown that (R)-LCM does not inhibit Ca^{2+} currents in hippocampal neurons [70] but whether (*S*)-LCM inhibits Ca^{2+} currents in sensory neurons is unknown. For these voltage-clamp experiments we chose a concentration of 10μM (*S*)-LCM, a value ~8 times the IC_{50} value calculated from Ca^{2+} imaging experiments, to assess potential off-target effects. A 30-min application with 10μM (*S*)-LCM did not inhibit low voltage-gated Ca^{2+} currents in DRGs (Supplementary Fig. 2A–B). In contrast, (*S*)-LCM inhibited high voltage-gated Ca^{2+} currents in DRGs by ~41% (Fig. 3A–D) without affecting channel activation (Fig. 3E) or inactivation (Fig. 3F, G). This level of inhibition is similar to what we observed with the CRMP2/CaV2.2 uncoupling peptide, but the latter required an overnight incubation [29]. By comparison, ω-conotoxin GVIA peptide, despite directly blocking the channel, inhibits DRG Ca^{2+} influx by ~34% at its IC_{50} [1]. Gabapentin, which targets trafficking of CaV2.2 by inhibiting the recycling of the channel [68], decreased DRG Ca^{2+} currents by only ~45% at a concentration of 1 mM, and required > 40 hours incubation to achieve this level of inhibition [31; 32]. Finally, since N-, P/Q- and R-type calcium currents can be inhibited by activation of GPCRs that are linked to $G_{i/o}$ (for a review, see [20]), we

tested if (*S*)-LCM affects G-protein inhibition of CaV2.2, which can be relieved by depolarization. (*S*)-LCM did not affect the ratio of currents between the pulses (Supplementary Fig. 2 C–D), ruling out involvement of G-proteins in its regulation of CaV2.2. These findings strengthen the hypothesis that (*S*)-LCM is an effective novel strategy for curbing Ca^{2+} currents and is likely superior to currently available clinically used CaV2.2 inhibitors.

Constellation pharmacology, a paradigm for 'fingerprinting' sensory neurons responsive to (S)-LCM treatment

The results obtained thus far demonstrate high synchronicity between (*S*)-LCM's inhibition of Cdk5-mediated CRMP2 phosphorylation and inhibition of Ca^{2+} influx via CaV2.2 in DRGs but do not the address the type of neuron targeted by (*S*)-LCM. To test this, we used the recently described phenotypic screening method termed constellation pharmacology [63; 64], which uses subtype-selective pharmacological agents to elucidate cell-specific combinations (constellations) of key signaling proteins that define specific cell types. The constellation pharmacology protocol consists of sequential challenges, applied 6-min apart, to test activity of Ca^{2+} permeable ligand-gated ion channels, metabotropic receptors and voltage-gated Ca^{2+} channels. At the end of each experiment, a membrane-depolarizing agent (i.e. KCl) is used to ensure neuronal viability; neurons that did not respond to this trigger were not analyzed. In each case the readout is a change in Ca^{2+} fluorescence. Typical responses to the challenges (Table 1) used are illustrated in Figure 4 (also see Supplementary Movies). Examples of typical Ca^{2+} traces of DRGs incubated with vehicle (0.002% DMSO) (Fig. 5A and Supplementary Fig. 3A) or (*S*)-LCM (10 μM) (Fig. 5B and Supplementary Fig. 3B) demonstrate the heterogeneity in responses. Importantly, consistent with our earlier data (Fig. 2), (*S*)-LCM reproducibly decreased the K^+-evoked Ca^{2+} influx despite being applied after several challenges of the constellation pharmacology protocol.

We applied the constellation pharmacology protocol to DRG neurons treated for 30 min with 10 μM (*S*)-LCM (n= 858) or 0.002% DMSO (vehicle, n=796) (Table 1). Data from 8 independent experiments were collected and the responses of each neuron to each constellation pharmacology trigger were analyzed. Only DRGs with responses >10% over the baseline fluorescence were considered in our analyses. We first asked if (*S*)-LCM treatment altered the overall competence of the neurons by assessing if the DRGs respond to the same number of agonist challenges, independently of which compound they responded to (Fig. 6A). In vehicle-treated DRGs, 26% of cells responded to KCl only (labeled as 0 in radar plot in Fig. 6A), 54 % responded to KCl plus 1 other trigger (labeled 1 in Fig. 6A), and ~16% responded to KCl plus 2 other triggers (2 in Fig 6A). The percent of neurons responding to more than 2 triggers was ≤ 3% (Supplementary Table 1). These percent responses were not altered by incubation with (*S*)-LCM (Fig. 6A, *red lines*), demonstrating that the drug does not affect the overall capacity of sensory neurons to respond to agonist challenges.

We next asked if (*S*)-LCM could change the *sensitivity* of sensory neurons to the different agonist challenges. We analyzed the percent of cells responding to a defined trigger, independently of any other trigger the cells may have responded to. In vehicle-treated DRGs,

the percent responders to the various triggers were: ~31% (Acetylcholine (Ach)), 15% (allyl isothiocyanate (AITC)), 11% ATP, 0.8% histamine, 6% menthol, and 40% capsaicin (Fig. 6B and Supplementary Table 1). (*S*)-LCM-treatment of DRGs decreased the percent responders to Ach (10%, $p<0.001$, z-test) and AITC (5.2 %, $p=0.05$), but increased the percent responders to menthol (26%, $p=0.005$) compared to control (Fig. 6B). The percent responders to ATP (6%, $p=0.516$), histamine (3 %, $p=0.284$) and capsaicin (35%, $p=0.336$) were not different between the conditions (Fig. 6B). These results demonstrate that (*S*)-LCM can target distinct neuronal populations, including those with decreased responsiveness and hence loss of functional acetylcholine receptors or transient receptor potential cation (TRPA1) channels (AITC responders), or those with increased responsiveness and hence a gain in expression of the cold sensor – functional transient receptor potential cation, subfamily M, member 8 (TRPM8) channels (menthol responder).

We further characterized the responses of the TRPM8 sensitive (i.e., menthol responding) neurons by challenging them with innocuous (17°C) or noxious (4°C) cold stimuli. (*S*)-LCM treatment increased the percent responders to the noxious cold stimulus compared to control, but the percent of neurons responding to the innocuous cold stimulus was not changed compared to control treated neurons (Fig. 6D). These results are consistent with the increased sensitivity of (*S*)-LCM treated sensory neurons to menthol (Fig. 6B).

In addition to the above classes, other major neuronal populations targeted by (*S*)-LCM were observed in our experiments (Fig. 6C and Supplementary Table 1). For instance, we noted that (*S*)-LCM decreased the percent of neurons responding to acetylcholine only (5% versus 20% in control, $p=0.023$) and AITC only (1% versus 6% in control, $p=0.05$) (Fig. 6C). Consistent with the earlier analyses, (*S*)-LCM increased the percent of neurons responding to menthol only (16% versus 2% in control, $p=0.05$) (Fig. 6C). Although, clear differences were observable in the populations responding to only KCl (34% versus 26% in control, $p=0.099$), Ach and capsaicin (2% versus 6% in control, $p=0.23$), or menthol and capsaicin (5% versus 0.5% in control, $p=0.682$), the low number of cells observed in these triggers combinations did not allow for statistical significance to be reached. Nevertheless, the results are in line with the overall decrease of percent of neurons responding to AITC or Ach (Fig. 6B, C) and the overall increase in percent of neurons responding to menthol (Fig. 6B, C) with (*S*)-LCM treatment. These results triangulate to the identification of a population of DRGs responding preferentially to Ach or AITC with (*S*)-LCM treatment.

(S)-lacosamide inhibits evoked Ca^{2+} influx in all classes of sensory neurons

The above analyses do not take into account the extent of inhibition of Ca^{2+} influx following each challenge. Therefore, here we analyzed peak Ca^{2+} responses of responders to the various triggers. Concurrent with the inhibition in K^+-evoked Ca^{2+} influx observed in single trigger experiments earlier (Fig. 2), (*S*)-LCM decreased K^+-evoked Ca^{2+} influx in a predictable way (~66% reduction compared to control, $p<0.001$) (Fig. 6E). Remarkably, compared to vehicle-treated neurons, the peak Ca^{2+} amplitude of (*S*)-LCM-treated DRGS were decreased for almost all triggers: 42% Ach ($p<0.001$); 44% AITC ($p=0.002$); 43% Menthol ($p<0.001$); or 60% capsaicin ($p<0.001$) (Fig. 6E). In contrast, the peak Ca^{2+}

amplitude of (*S*)-LCM-treated DRGs to histamine (p=0.08) or ATP (p=0.22) was not different from control (Fig. 6E).

We next asked if the inhibition of K^+-evoked Ca^{2+} influx by (*S*)-LCM could be echoed in certain functional classes identified in our earlier analyses. We investigated the average peak Ca^{2+} response to KCl stimulation of neurons that responded to a trigger, independent of any other compounds they responded to. In vehicle-treated DRGs, the average peak Ca^{2+} response to KCl was higher by 122% and 168% for cells responding to ATP and or capsaicin, respectively ($p<0.001$) and lower by 20% for cells responding to Ach ($p<0.001$) (Fig. 6G). In contrast, in (*S*)-LCM-treated DRGs, the average peak Ca^{2+} response to KCl was lower for all triggers compared to control cells total population but unchanged between functional classes of neurons (Fig. 6G, *right columns*). Additionally, (*S*)-LCM decreased the peak Ca^{2+} response to both innocuous and noxious cold stimuli (Fig. 6F). These results illustrate the heterogeneity of sensory neurons in their capacity to respond to a membrane-depolarization.

To obtain a more precise understanding of the preferential targeting of (*S*)-LCM effect on Ca^{2+} influx after depolarization, we analyzed the peak KCl response of the neuronal subpopulations identified in Fig. 6C. Ca^{2+} influx following depolarization was decreased by (*S*)-LCM treatment compared to control for all trigger combinations except Ach only (p=0.088), AITC only (p=0.075), and menthol/capsaicin together (p=0.77) (Fig. 6H). Together, these results demonstrate that (*S*)-LCM (*i*) identifies distinct classes of neurons and (*ii*) decreases peak Ca^{2+} responses of specific receptor agonists.

Size distribution of neuronal populations targeted by (S)-lacosamide

DRG neurons are heterogeneous in size [30]. While cell size approximates the functional class of DRG neurons, it is not an absolute predictor of functional type of neuron. Having identified classes of neurons that respond differently to the triggers, we next asked if the some of these changes could be due to the size heterogeneity of the neurons. There were no differences in the numbers of cells across different cell sizes between vehicle- or (*S*)-LCM-treated neurons (Fig. 7A). In cells responding to KCl only, (*S*)-LCM treatment increased the number of cells of a size between 500–699μm^2 or >1000μm^2 (Fig. 7B). In cells responding to 1 trigger, there were no differences in the numbers of cells across different cell sizes between vehicle- or (*S*)-LCM-treated neurons (Fig. 7C). Similarly, no changes were observed if cell size was examined for cells responding to more than 1 trigger (data not shown). Among the capsaicin responders, there were no differences in the numbers of cells across different cell sizes between vehicle- or (*S*)-LCM-treated neurons (Fig. 7D). Among the AITC responding neurons, whose overall percent was decreased by (*S*)-LCM, we noted a decrease in the number of neurons with a size between 500–699μm^2 (Fig. 7E). Finally, since (*S*)-LCM increased the percent of menthol responsive neurons (Fig. 6B), we analyzed if a specific neuron size class among the menthol responding cells was enriched by the (*S*)-LCM treatment. However, no such enrichment was noted (Fig. 7F). We did not observe specific size class enrichment in cells responding to innocuous cold stimuli (Supplementary Fig. 3C). In contrast, we noted an increase in the number of small- to medium-sized neurons (i.e., those between 0–399μm^2, 500–599μm^2, and 700–849μm^2) among the (*S*)-LCM-treated

neurons responding to 4°C (Supplementary Fig. 3D). These results highlight that (*S*)-LCM targets, without discrimination, all neuronal size classes except for small sized neurons responding to AITC. The constellation pharmacology experiments identify distinct neuron classes and size following (*S*)-LCM treatment and may contribute to a better understanding of how this drug may achieve antinociceptive efficacy.

(S)-lacosamide reverses post-surgical pain

Targeting CaV2.2 is a useful strategy in this model as (*i*) the α2δ-targeted compound gabapentin is effective in reversing mechanical hyperalgesia [26], and (ii) ziconotide presumably decreased patient controlled analgesia morphine equivalent consumption and visual analog pain intensity scores [3]. Therefore, we tested the anociceptive potential of (*S*)-LCM on thermal hyperalgesia and tactile allodynia induced by an incision of the plantaris muscle of the rat hind paw, a model of postoperative surgical pain [7].

An incision of the rat plantaris muscle led to a reduction of the paw withdrawal threshold (mechanical allodynia) and of paw withdrawal latency (thermal hyperalgesia) (Fig. 9). Both nociceptive responses peaked within 24 h after surgery and were maintained during the 5 to 6 h experimental period in vehicle-treated animals. Spinal administration of (*S*)-LCM blocked the development of mechanical hypersensitivity for at least 4.5 h (Fig. 9A, B), and thermal hypersensitivity was suppressed during the course of the experiment (Fig. 9C). We determined the area under the curve (AUC) to assess effects over the full experimental duration. AUC analysis confirmed the reversal of mechanical allodynia and thermal hyperalgesia compared to sham-injured vehicle-treated injured animals (Fig. 9B, D). Our previous findings reporting similar relief from post-surgical pain behaviors with a membrane-tethered peptide that uncoupled the CRMP2/CaV2.2 interaction [29] and these data support the idea that targeting CRMP2, specifically phosphorylation in this study, is a rationale new therapeutic strategy for post-surgical pain.

(S)-lacosamide reverses neuropathic pain

Our earlier findings from (*S*)-LCM–treated DRG neurons identified neuron classes with diminished responsiveness to Ach, diminished peak Ca^{2+} response to capsaicin, and an increase responsiveness to menthol (Fig. 6B, D). All three of these changes have been implicated in neuropathic pain. For instance, Ach receptors have been implicated in nociception following a neuropathic injury [43; 46]. Similarly, capsaicin responding neurons are linked to neuropathic pain [33; 46; 81]. Furthermore, menthol receptor (TRPM8) activation was reported to provide relief of neuropathic pain [51]. In addition to these findings, the CRMP2 phophorylating kinase Cdk5 is dysregulated during neuropathic suggesting that CRMP2 phosphorylation might itself be dysregulated [41]. We hypothesized that (*S*)-LCM treatment could result in a reversal of nociception of neuropathic pain by inhibiting CRMP2 phosphorylation. To test this hypothesis, (*S*)-LCM was evaluated for efficacy in the spared nerve injury (SNI) model [18] of neuropathic pain. SNI significantly reduced paw withdrawal thresholds (PWTs) 7–9 days post injury (Fig. 10A). Spinal administration of (*S*)-LCM significantly increased PWTs over post-baseline SNI-values at 2–4 hr post-injection (Fig. 10A). In contrast, vehicle-treatment did not increase PWTs compared to post-baseline SNI values (Fig. 10A). We also determined the AUC to assess

effects over the full experimental duration. AUC analysis confirmed the reversal of mechanical allodynia compared to vehicle-treated injured animals (Fig. 10B).

We also used the spinal nerve ligation (SNL) model of neuropathic pain to evaluate the potential of (*S*)-LCM to reverse nociception. SNL injury efficiently reduced PWTs (mechanical allodynia, Fig. 10A) and paw withdrawal latency (PWL, thermal hyperalgesia, Fig. 10B) 7 days post injury. Spinal administration of (*S*)-LCM significantly increased both PWTs (Fig. 10A) and PWL (Fig. 10B) for the entire course of the experiment (4 hours). AUC analysis confirmed the reversal of mechanical allodynia (Fig. 10C) and thermal hyperalgesia (Fig. 10D) compared to vehicle-treated injured animals.

(S)-lacosamide does not produce motor impairment or paralysis in naïve rats

Finally, (*S*)-LCM was evaluated for typical motor deficits or sedation reported with N-type calcium channel blocking compounds [3]. Rats were trained to walk on a rotating rod with a maximal cutoff time of 180 seconds before administration of (*S*)-LCM (3μg/5μL i.th) or vehicle (0.9% sodium chloride). The mean baseline latency for all animals was 180 seconds. Vehicle-treated animals remained on the rotarod for an average of 180 seconds at each time point over the course of 240 minutes. Animals treated with (*S*)-LCM (3μg/5μL i.th.) remained on the rotarod for an average of 178 seconds over the course of 240 minutes (Fig. 11). These results demonstrate that (*S*)-LCM treatment does not result in sedation or motoric impairment. Thus, using (*S*)-LCM in vivo is a safe strategy to target voltage gated N-type Ca^{2+} channels and reverse chronic pain.

DISCUSSION

The data reported here demonstrate the utility of a small molecule targeting CRMP2 phosphorylation to specifically control CaV2.2 activity, highlight the use of constellation pharmacology to triangulate neuronal subclasses responsive to various triggers that are changed following drug treatment and provide validation of CRMP2 as a new *druggable* target for postoperative and neuropathic pain.

CaV2.2 is a high-value target for the treatment of chronic pain and drugs targeting this channel have demonstrated clinical efficacy in modulation of pain [59; 69]. These drugs are, however, accompanied by a high incidence of side effects [4; 59; 69]. Intrathecal administration of the ω-conotoxin MVIIA provoked undesirable effects in more than 95% of patients where dizziness was the most reported adverse effect [4; 59; 69]. Off-target effects are likely due to widespread functions associated with CaV2.2, especially in modulating synaptic transmission at supraspinal sites [23]. In neuropathic pain, CaV2.2 expression in laminae I and II of the dorsal horn of the spinal cord, is increased [15]. Thus, the synapses from the small diameter DRGs, responsible for nociceptive signaling, are enriched in CaV2.2 [15]. Expression of CRMP2 [15; 35], as well as that of its phosphorylating kinase Cdk5, is increased in pain states [35; 41; 49; 83]. These findings suggest the possibility that CRMP2 phosphorylation is also likely increased in pain states. Finally, we reported that Cdk5 phosphorylation of CRMP2 strengthens its interactions with CaV2.2 and allows increased activity of CaV2.2 [10]. Thus, restricting CRMP2 phosphorylation, which may be

a pathologic event in neuropathic pain, using the small molecule (*S*)-LCM [47], appears to be a rational novel strategy for developing blockers for pain.

In contrast to other drugs currently available for targeting CaV2.2, (*S*)-LCM may offer some advantages. *First*, (*S*)-LCM does not directly target CaV2.2 but does so indirectly by inhibiting Cdk5-mediated CRMP2 phosphorylation to inhibit the CRMP2-CaV2.2 interaction which leads to a reduction in Ca^{2+} influx – this is a completely new mechanism for targeting CaV2.2. *Second*, despite being an indirect 'blocker' of Ca^{2+} influx, (*S*)-LCM provides improved efficacy compared to TROX-1, a small-molecule, state-dependent blocker of CaV2 channels [1] as well as a membrane-tethered CRMP2 peptide that uncouples the CRMP2-CaV2.2 interaction that we recently reported [28]. *Third*, (*S*)-LCM has a faster (within 30 min) onset of action compared to gabapentin, which targets trafficking of CaV2.2 [68] but requires > 40 hours incubation to achieve its effects [31; 32] or the CRMP2-CaV2.2 interaction uncoupling peptide which requires >24 hours for its efficacy [28]. Lastly, (*S*)-LCM does not alter any biophysical properties of CaV2.2.

Recently, CRMP2 was identified as a nociceptor-enriched gene [66]. To characterize precisely the neuronal classes affected by (*S*)-LCM, we used the recently described constellation pharmacology approach [64; 65]. This is a cell-based high content phenotypic-screening strategy using a series of agonists to dissect phenotypic neuronal classes [63]. Among the (*S*)-LCM-treated neurons we observed a decrease in the percent of cells responding to AITC or Ach and an increase in the percent of cells responding to menthol (Fig. 7B). Notably, the receptors/channels associated with these triggers have been linked to pain [42; 51; 73]. Activation of the transient receptor potential ankyrin 1 (TRPA1, activated by AITC) was found to be sufficient to produce allodynia [16] while activation of TRPM8 may be either pro- or antinociceptive depending on the assay system studied. For example, oxaliplatin-induced cold allodynia was unaffected in TRPM8 null animals or by the TRPM8-selective inhibitors [19]. Proudfoot et al., demonstrated that activation of TRPM8 in a subpopulation of sensory afferents elicits analgesia in neuropathic and other chronic pain models in rats [51]. AMG2850, a potent antagonist of TRPM8, was not effective in rat models of inflammatory mechanical hypersensitivity or neuropathic tactile allodynia [40]. On the other hand, AMG 1161, a TRPM8 antagonist, was effective in blocking facial and hindpaw allodynia induced by application of a TRPM8 agonist (i.e., icillin) onto the dura mater of rats [12], suggesting a role of this channel in pronociceptive actions to promote migraine pain. Another salient finding from these experiments was the observation that (*S*)-LCM decreases the peak Ca^{2+} response to Ach, AITC, menthol, capsaicin and KCl (Fig. 7D). These pharmacology triggers activate ligand-gated (triggers nicotinic acetylcholine receptor, TRPM8, TRPA1, TRPV1) and voltage-gated Ca^{2+} channels [65]. Histamine and ATP peak responses where not altered by (*S*)-LCM treatment (Fig. 7D). Interestingly, the receptors activated by these compounds are coupled to G-proteins that indirectly increase Ca^{2+} intracellular concentration through downstream signaling pathways, thus triggering the release of Ca^{2+} from the endoplasmic reticulum [39; 60]. Therefore, (*S*)-LCM treatment appears to have an inhibitory effect *only* on ligand- and voltage-gated ion channels but not on G protein coupled receptors (GPCRs). While CRMP2 controls trafficking of ligand- and voltage-gated ion channels [8; 9; 11; 21], this is the first demonstration that CRMP2 is not coupled to GPCRs. Thus, these findings identify the potential of (*S*)-LCM to affect the

activity of ligand gated ion channels including, TRPV1, TRPA1, TRPM8 or nicotinic acetylcholine receptor.

Our results point to a critical role for CRMP2 phosphorylation in the etiology of neuropathic pain but how this may occur is uncertain. Following nerve injury, a remodeling of the synaptic network is thought to underlie the development of chronic pain [13; 34; 61]. The length and diameter of dendritic spines in the spinal cord, reportedly increases, together with their density along the dendrites [61; 62]. This correlates with an increase of the firing rate of the neurons in the spinal cord [62] and a change of shape of the synapses towards a mushroom phenotype [61; 62]. Additionally, the mushroom-shaped dendritic spines were observed to promote the propagation of excitatory potentials by the attenuation of inhibitory input resulting in facilitation of pain signal transmission [61]. Inhibiting a small GTPase involved in dendritic spine development, reversed the phenotype of dendritic spines, decreased the firing rate of spinal cord neurons and produced analgesia [62]. CRMP2 has been described for its fundamental role in neurite outgrowth and dendritic development [78; 82]. More specifically, defects in CRMP2 phosphorylation by Cdk5, induced a severe abnormal dendritic pattern preventing dendritic projections in the cortex [82]. CRMP2 expression can control the size of synaptic buttons, located at the distal end of the dendritic spines [9]. (*S*)-LCM inhibition of both CRMP2-dependent neurite outgrowth [78] and CRMP2 phosphorylation by Cdk5 suggests that the use of this small molecule could prevent/reverse the development of chronic pain by inhibiting the positive input of CRMP2 into dendritic spine development.

Slight differences in kinetics were observed for (*S*)-LCM mediated reversal of pain behaviors: onset of reversal of hypersensitivity was ~30 min for postsurgical pain and about 2 hr for neuropathic pain with efficacy for ~4 hr in both models. The time course observed is nevertheless consistent with pharmacokinetic data from (*R*)-LCM, which, in humans, has a reported half-life of ~3 hr, follows linear plasma concentration profiles with 100% oral bioavailability at doses up to 20 mg/kg, has a favorable brain to plasma partition coefficient (0.55), and reaches a peak concentration at ~40 min following an oral dose [38]. We expect that the enantiomer, (*S*)-LCM will show similar favorable drug-like qualities and appropriate safety. Lack of neurobehavioral toxicity observed in rats in our experiments now sets the stage for additional testing so as to justify rapid advancement and evaluation of this molecule in clinical trials representing an entirely new mechanism for treatment of postsurgical and neuropathic pain in humans.

Currently available drugs for chronic pain directly targeting CaV2.2 provide are moderately effective but encumbered with a high incidence of adverse effects [59; 69]. Our results demonstrate that indirect targeting of CaV2.2 may offer an advantage as (*S*)-LCM, which inhibits CRMP2 phosphorylation by Cdk5 to curb CaV2.2 activity, is antinociceptive in preclinical models of postsurgical and neuropathic pain. Equally important, we predict that (*S*)-LCM, being an enantiomer of a clinically used drug, will be amenable to a rapid development path for the treatment of pain, highlighting the utility of repurposing clinical drugs based on a deeper understanding of their mechanism(s) of action. Additionally, data from constellation pharmacology permitted the phenotypic classification of neuronal

subtypes altered by (*S*)-LCM treatment, stressing the utility of this approach as a strategy for drug discovery and side effect profiling.

Supplementary Material

Refer to Web version on PubMed Central for supplementary material.

Acknowledgments

This work was supported by a Career Development Award from the Arizona Health Science Center to M.K., a National Scientist Development grant SDG5280023 from the American Heart Association and a Neurofibromatosis New Investigator Award NF1000099 from the Department of Defense Congressionally Directed Military Medical Research and Development Program to R.K. A.M. was partially supported by a Young Investigator Award from the Children's Tumor Foundation. L.A.C. was partially supported by the Flinn Scholarship, and grants from the University of Arizona's Undergraduate Biology Research Program, the Undergraduate Honors College, and the Neuroscience and Cognitive Science Undergraduate fund.

REFERENCES

1. Abbadie C, McManus OB, Sun SY, Bugianesi RM, Dai G, Haedo RJ, Herrington JB, Kaczorowski GJ, Smith MM, Swensen AM, Warren VA, Williams B, Arneric SP, Eduljee C, Snutch TP, Tringham EW, Jochnowitz N, Liang A, Euan MacIntyre D, McGowan E, Mistry S, White VV, Hoyt SB, London C, Lyons KA, Bunting PB, Volksdorf S, Duffy JL. Analgesic effects of a substituted N-triazole oxindole (TROX-1), a state-dependent, voltage-gated calcium channel 2 blocker. J Pharmacol Exp Ther. 2010; 334(2):545–555. [PubMed: 20439438]
2. Anichtchik OV, Kaslin J, Peitsaro N, Scheinin M, Panula P. Neurochemical and behavioural changes in zebrafish Danio rerio after systemic administration of 6-hydroxydopamine and 1-methyl-4-phenyl-1,2,3,6-tetrahydropyridine. Journal of neurochemistry. 2004; 88(2):443–453. [PubMed: 14690532]
3. Atanassoff PG, Hartmannsgruber MW, Thrasher J, Wermeling D, Longton W, Gaeta R, Singh T, Mayo M, McGuire D, Luther RR. Ziconotide, a new N-type calcium channel blocker, administered intrathecally for acute postoperative pain. Regional anesthesia and pain medicine. 2000; 25(3):274–278. [PubMed: 10834782]
4. Backonja M, Glanzman RL. Gabapentin dosing for neuropathic pain: evidence from randomized, placebo-controlled clinical trials. Clin Ther. 2003; 25(1):81–104. [PubMed: 12637113]
5. Ben-Menachem E, Biton V, Jatuzis D, Abou-Khalil B, Doty P, Rudd GD. Efficacy and safety of oral lacosamide as adjunctive therapy in adults with partial-onset seizures. Epilepsia. 2007; 48(7):1308–1317. [PubMed: 17635557]
6. Braithwaite VA, Boulcott P. Pain perception, aversion and fear in fish. Dis Aquat Organ. 2007; 75(2):131–138. [PubMed: 17578252]
7. Brennan TJ, Vandermeulen EP, Gebhart GF. Characterization of a rat model of incisional pain. Pain. 1996; 64(3):493–501. [PubMed: 8783314]
8. Brittain JM, Duarte DB, Wilson SM, Zhu W, Ballard C, Johnson PL, Liu N, Xiong W, Ripsch MS, Wang Y, Fehrenbacher JC, Fitz SD, Khanna M, Park CK, Schmutzler BS, Cheon BM, Due MR, Brustovetsky T, Ashpole NM, Hudmon A, Meroueh SO, Hingtgen CM, Brustovetsky N, Ji RR, Hurley JH, Jin X, Shekhar A, Xu XM, Oxford GS, Vasko MR, White FA, Khanna R. Suppression of inflammatory and neuropathic pain by uncoupling CRMP-2 from the presynaptic Ca(2)(+) channel complex. Nature medicine. 2011; 17(7):822–829.
9. Brittain JM, Piekarz AD, Wang Y, Kondo T, Cummins TR, Khanna R. An atypical role for collapsin response mediator protein 2 (CRMP-2) in neurotransmitter release via interaction with presynaptic voltage-gated calcium channels. The Journal of biological chemistry. 2009; 284(45):31375–31390. [PubMed: 19755421]
10. Brittain JM, Wang Y, Eruvwetere O, Khanna R. Cdk5-mediated phosphorylation of CRMP-2 enhances its interaction with CaV2.2. FEBS letters. 2012; 586(21):3813–3818. [PubMed: 23022559]

11. Brustovetsky T, Pellman JJ, Yang XF, Khanna R, Brustovetsky N. Collapsin response mediator protein 2 (CRMP2) interacts with N-methyl-D-aspartate (NMDA) receptor and Na+/Ca2+ exchanger and regulates their functional activity. The Journal of biological chemistry. 2014; 289(11):7470–7482. [PubMed: 24474686]
12. Burgos-Vega CC, Ahn DD, Bischoff C, Wang W, Horne D, Wang J, Gavva N, Dussor G. Meningeal transient receptor potential channel M8 activation causes cutaneous facial and hindpaw allodynia in a preclinical rodent model of headache. Cephalalgia : an international journal of headache. 2016; 36(2):185–193. [PubMed: 25944818]
13. Chien SQ, Li C, Li H, Xie W, Pablo CS, Zhang JM. Sympathetic Fiber Sprouting in Chronically Compressed Dorsal Root Ganglia Without Peripheral Axotomy. J Neuropathic Pain Symptom Palliation. 2005; 1(1):19–23. [PubMed: 17387381]
14. Choe W, Messinger RB, Leach E, Eckle VS, Obradovic A, Salajegheh R, Jevtovic-Todorovic V, Todorovic SM. TTA-P2 is a potent and selective blocker of T-type calcium channels in rat sensory neurons and a novel antinociceptive agent. MolPharmacol. 2011; 80(5):900–910.
15. Cizkova D, Marsala J, Lukacova N, Marsala M, Jergova S, Orendacova J, Yaksh TL. Localization of N-type Ca2+ channels in the rat spinal cord following chronic constrictive nerve injury. Experimental brain research. 2002; 147(4):456–463. [PubMed: 12444477]
16. Cruz-Orengo L, Dhaka A, Heuermann RJ, Young TJ, Montana MC, Cavanaugh EJ, Kim D, Story GM. Cutaneous nociception evoked by 15-delta PGJ2 via activation of ion channel TRPA1. Mol Pain. 2008; 4:30. [PubMed: 18671867]
17. Curtright A, Rosser M, Goh S, Keown B, Wagner E, Sharifi J, Raible DW, Dhaka A. Modeling nociception in zebrafish: a way forward for unbiased analgesic discovery. PloS one. 2015; 10(1):e0116766. [PubMed: 25587718]
18. Decosterd I, Woolf CJ. Spared nerve injury: an animal model of persistent peripheral neuropathic pain. Pain. 2000; 87(2):149–158. [PubMed: 10924808]
19. Deuis JR, Zimmermann K, Romanovsky AA, Possani LD, Cabot PJ, Lewis RJ, Vetter I. An animal model of oxaliplatin-induced cold allodynia reveals a crucial role for Nav1.6 in peripheral pain pathways. Pain. 2013; 154(9):1749–1757. [PubMed: 23711479]
20. Dolphin AC. G protein modulation of voltage-gated calcium channels. Pharmacological reviews. 2003; 55(4):607–627. [PubMed: 14657419]
21. Dustrude ET, Wilson SM, Ju W, Xiao Y, Khanna R. CRMP2 protein SUMOylation modulates NaV1.7 channel trafficking. The Journal of biological chemistry. 2013; 288(34):24316–24331. [PubMed: 23836888]
22. Errington AC, Stohr T, Heers C, Lees G. The investigational anticonvulsant lacosamide selectively enhances slow inactivation of voltage-gated sodium channels. Molecular pharmacology. 2008; 73(1):157–169. [PubMed: 17940193]
23. Evans RM, Zamponi GW. Presynaptic Ca2+ channels--integration centers for neuronal signaling pathways. Trends in neurosciences. 2006; 29(11):617–624. [PubMed: 16942804]
24. Feldman P, Khanna R. Challenging the catechism of therapeutics for chronic neuropathic pain: Targeting CaV2.2 interactions with CRMP2 peptides. Neuroscience letters. 2013; 557(Pt A):27–36. [PubMed: 23831344]
25. Feng ZP, Hamid J, Doering C, Bosey GM, Snutch TP, Zamponi GW. Residue Gly1326 of the N-type calcium channel alpha 1B subunit controls reversibility of omega-conotoxin GVIA and MVIIA block. The Journal of biological chemistry. 2001; 276(19):15728–15735. [PubMed: 11279062]
26. Field MJ, Holloman EF, McCleary S, Hughes J, Singh L. Evaluation of gabapentin and S-(+)-3-isobutylgaba in a rat model of postoperative pain. The Journal of pharmacology and experimental therapeutics. 1997; 282(3):1242–1246. [PubMed: 9316831]
27. Finnerup NB, Attal N, Haroutounian S, McNicol E, Baron R, Dworkin RH, Gilron I, Haanpaa M, Hansson P, Jensen TS, Kamerman PR, Lund K, Moore A, Raja SN, Rice AS, Rowbotham M, Sena E, Siddall P, Smith BH, Wallace M. Pharmacotherapy for neuropathic pain in adults: a systematic review and meta-analysis. Lancet Neurol. 2015; 14(2):162–173. [PubMed: 25575710]
28. Francois-Moutal L, Wang Y, Moutal A, Cottier KE, Melemedjian OK, Yang X, Wang Y, Ju W, Largent-Milnes TM, Khanna M, Vanderah TW, Khanna R. A membrane-delimited N-

myristoylated CRMP2 peptide aptamer inhibits CaV2.2 trafficking and reverses inflammatory and post-operative pain behaviors. Pain. 2015

29. Francois-Moutal L, Wang Y, Moutal A, Cottier KE, Melemedjian OK, Yang X, Wang Y, Ju W, Largent-Milnes TM, Khanna M, Vanderah TW, Khanna R. A membrane-delimited N-myristoylated CRMP2 peptide aptamer inhibits CaV2.2 trafficking and reverses inflammatory and postoperative pain behaviors. Pain. 2015; 156(7):1247–1264. [PubMed: 25782368]
30. Harper AA, Lawson SN. Conduction velocity is related to morphological cell type in rat dorsal root ganglion neurones. The Journal of physiology. 1985; 359:31–46. [PubMed: 3999040]
31. Heblich F, Tran Van Minh A, Hendrich J, Watschinger K, Dolphin AC. Time course and specificity of the pharmacological disruption of the trafficking of voltage-gated calcium channels by gabapentin. Channels (Austin). 2008; 2(1):4–9. [PubMed: 18690052]
32. Hendrich J, Van Minh AT, Heblich F, Nieto-Rostro M, Watschinger K, Striessnig J, Wratten J, Davies A, Dolphin AC. Pharmacological disruption of calcium channel trafficking by the alpha2delta ligand gabapentin. Proceedings of the National Academy of Sciences of the United States of America. 2008; 105(9):3628–3633. [PubMed: 18299583]
33. Hirai T, Enomoto M, Kaburagi H, Sotome S, Yoshida-Tanaka K, Ukegawa M, Kuwahara H, Yamamoto M, Tajiri M, Miyata H, Hirai Y, Tominaga M, Shinomiya K, Mizusawa H, Okawa A, Yokota T. Intrathecal AAV serotype 9-mediated delivery of shRNA against TRPV1 attenuates thermal hyperalgesia in a mouse model of peripheral nerve injury. Mol Ther. 2014; 22(2):409–419. [PubMed: 24322332]
34. Hu J, Mata M, Hao S, Zhang G, Fink DJ. Central sprouting of uninjured small fiber afferents in the adult rat spinal cord following spinal nerve ligation. The European journal of neuroscience. 2004; 20(7):1705–1712. [PubMed: 15379991]
35. Kamiya Y, Saeki K, Takiguchi M, Funakoshi K. CDK5, CRMP2 and NR2B in spinal dorsal horn and dorsal root ganglion have different role in pain signaling between neuropathic pain model and inflammatory pain model. European Journal of Anaesthesiology. 2013; 30:214–214.
36. Kim C, Jeon D, Kim YH, Lee CJ, Kim H, Shin HS. Deletion of N-type Ca2+ channel Cav2.2 results in hyperaggressive behaviors in mice. JBiolChem. 2008
37. Kim C, Jun K, Lee T, Kim SS, McEnery MW, Chin H, Kim HL, Park JM, Kim DK, Jung SJ, Kim J, Shin HS. Altered nociceptive response in mice deficient in the alpha(1B) subunit of the voltage-dependent calcium channel. MolCell Neurosci. 2001; 18(2):235–245.
38. Koo TS, Kim SJ, Ha DJ, Baek M, Moon H. Pharmacokinetics, brain distribution, and plasma protein binding of the antiepileptic drug lacosamide in rats. Archives of pharmacal research. 2011; 34(12):2059–2064. [PubMed: 22210031]
39. Lee KC, Chang HT, Chou KJ, Tang KY, Wang JL, Lo YK, Huang JK, Chen WC, Su W, Law YP, Jan CR. Mechanism underlying histamine-induced intracellular Ca2+ movement in PC3 human prostate cancer cells. Pharmacol Res. 2001; 44(6):547–552. [PubMed: 11735364]
40. Lehto SG, Weyer AD, Zhang M, Youngblood BD, Wang J, Wang W, Kerstein PC, Davis C, Wild KD, Stucky CL, Gavva NR. AMG2850, a potent and selective TRPM8 antagonist, is not effective in rat models of inflammatory mechanical hypersensitivity and neuropathic tactile allodynia. Naunyn-Schmiedeberg's archives of pharmacology. 2015; 388(4):465–476.
41. Li K, Zhao GQ, Li LY, Wu GZ, Cui SS. Epigenetic upregulation of Cdk5 in the dorsal horn contributes to neuropathic pain in rats. Neuroreport. 2014; 25(14):1116–1121. [PubMed: 25055140]
42. Liu B, Fan L, Balakrishna S, Sui A, Morris JB, Jordt SE. TRPM8 is the principal mediator of menthol-induced analgesia of acute and inflammatory pain. Pain. 2013; 154(10):2169–2177. [PubMed: 23820004]
43. Luo S, Zhangsun D, Harvey PJ, Kaas Q, Wu Y, Zhu X, Hu Y, Li X, Tsetlin VI, Christensen S, Romero HK, McIntyre M, Dowell C, Baxter JC, Elmslie KS, Craik DJ, McIntosh JM. Cloning, synthesis, and characterization of alphaO-conotoxin GeXIVA, a potent alpha9alpha10 nicotinic acetylcholine receptor antagonist. Proceedings of the National Academy of Sciences of the United States of America. 2015; 112(30):E4026–E4035. [PubMed: 26170295]
44. McGivern JG. Ziconotide: a review of its pharmacology and use in the treatment of pain. Neuropsychiatric disease and treatment. 2007; 3(1):69–85. [PubMed: 19300539]

45. Mintz IM, Venema VJ, Swiderek KM, Lee TD, Bean BP, Adams ME. P-type calcium channels blocked by the spider toxin omega-Aga-IVA. Nature. 1992; 355(6363):827–829. [PubMed: 1311418]
46. Moalem G, Grafe P, Tracey DJ. Chemical mediators enhance the excitability of unmyelinated sensory axons in normal and injured peripheral nerve of the rat. Neuroscience. 2005; 134(4):1399–1411. [PubMed: 16039795]
47. Moutal A, Francois-Moutal L, Perez-Miller S, Cottier K, Chew LA, Yeon SK, Dai J, Park KD, Khanna M, Khanna R. (S)-Lacosamide Binding to Collapsin Response Mediator Protein 2 (CRMP2) Regulates CaV2.2 Activity by Subverting Its Phosphorylation by Cdk5. Molecular neurobiology. 2015
48. Newcomb R, Szoke B, Palma A, Wang G, Chen X, Hopkins W, Cong R, Miller J, Urge L, Tarczy-Hornoch K, Loo JA, Dooley DJ, Nadasdi L, Tsien RW, Lemos J, Miljanich G. Selective peptide antagonist of the class E calcium channel from the venom of the tarantula Hysterocrates gigas. Biochemistry. 1998; 37(44):15353–15362. [PubMed: 9799496]
49. Pareek TK, Keller J, Kesavapany S, Pant HC, Iadarola MJ, Brady RO, Kulkarni AB. Cyclin-dependent kinase 5 activity regulates pain signaling. Proceedings of the National Academy of Sciences of the United States of America. 2006; 103(3):791–796. [PubMed: 16407116]
50. Pexton T, Moeller-Bertram T, Schilling JM, Wallace MS. Targeting voltage-gated calcium channels for the treatment of neuropathic pain: a review of drug development. Expert opinion on investigational drugs. 2011; 20(9):1277–1284. [PubMed: 21740292]
51. Proudfoot CJ, Garry EM, Cottrell DF, Rosie R, Anderson H, Robertson DC, Fleetwood-Walker SM, Mitchell R. Analgesia mediated by the TRPM8 cold receptor in chronic neuropathic pain. Current biology : CB. 2006; 16(16):1591–1605. [PubMed: 16920620]
52. Rauck RL, Shaibani A, Biton V, Simpson J, Koch B. Lacosamide in painful diabetic peripheral neuropathy: a phase 2 double-blind placebo-controlled study. The Clinical journal of pain. 2007; 23(2):150–158. [PubMed: 17237664]
53. Rauck RL, Wallace MS, Burton AW, Kapural L, North JM. Intrathecal ziconotide for neuropathic pain: a review. Pain practice : the official journal of World Institute of Pain. 2009; 9(5):327–337. [PubMed: 19682321]
54. Schmidtko A, Lotsch J, Freynhagen R, Geisslinger G. Ziconotide for treatment of severe chronic pain. Lancet. 2010; 375(9725):1569–1577. [PubMed: 20413151]
55. Scott DA, Wright CE, Angus JA. Actions of intrathecal omega-conotoxins CVID, GVIA, MVIIA, and morphine in acute and neuropathic pain in the rat. EurJPharmacol. 2002; 451(3):279–286. %20;
56. Sheets PL, Heers C, Stoehr T, Cummins TR. Differential block of sensory neuronal voltage-gated sodium channels by lacosamide [(2R)-2-(acetylamino)-N-benzyl-3-methoxypropanamide], lidocaine, and carbamazepine. The Journal of pharmacology and experimental therapeutics. 2008; 326(1):89–99. [PubMed: 18378801]
57. Skov MJ, Beck JC, de Kater AW, Shopp GM. Nonclinical safety of ziconotide: an intrathecal analgesic of a new pharmaceutical class. International journal of toxicology. 2007; 26(5):411–421. [PubMed: 17963128]
58. Sneddon LU. Trigeminal somatosensory innervation of the head of a teleost fish with particular reference to nociception. Brain research. 2003; 972(1–2):44–52. [PubMed: 12711077]
59. Staats PS, Yearwood T, Charapata SG, Presley RW, Wallace MS, Byas-Smith M, Fisher R, Bryce DA, Mangieri EA, Luther RR, Mayo M, McGuire D, Ellis D. Intrathecal ziconotide in the treatment of refractory pain in patients with cancer or AIDS: a randomized controlled trial. JAMA : the journal of the American Medical Association. 2004; 291(1):63–70. [PubMed: 14709577]
60. Svichar N, Shmigol A, Verkhratsky A, Kostyuk P. ATP induces Ca2+ release from IP3-sensitive Ca2+ stores exclusively in large DRG neurones. Neuroreport. 1997; 8(7):1555–1559. [PubMed: 9189891]
61. Tan AM, Choi JS, Waxman SG, Hains BC. Dendritic spine remodeling after spinal cord injury alters neuronal signal processing. J Neurophysiol. 2009; 102(4):2396–2409. [PubMed: 19692517]

62. Tan AM, Stamboulian S, Chang YW, Zhao P, Hains AB, Waxman SG, Hains BC. Neuropathic pain memory is maintained by Rac1-regulated dendritic spine remodeling after spinal cord injury. The Journal of neuroscience : the official journal of the Society for Neuroscience. 2008; 28(49):13173–13183. [PubMed: 19052208]

63. Teichert RW, Memon T, Aman JW, Olivera BM. Using constellation pharmacology to define comprehensively a somatosensory neuronal subclass. Proceedings of the National Academy of Sciences of the United States of America. 2014; 111(6):2319–2324. [PubMed: 24469798]

64. Teichert RW, Schmidt EW, Olivera BM. Constellation pharmacology: a new paradigm for drug discovery. Annu Rev Pharmacol Toxicol. 2015; 55:573–589. [PubMed: 25562646]

65. Teichert RW, Smith NJ, Raghuraman S, Yoshikami D, Light AR, Olivera BM. Functional profiling of neurons through cellular neuropharmacology. Proceedings of the National Academy of Sciences of the United States of America. 2012; 109(5):1388–1395. [PubMed: 22307590]

66. Thakur M, Crow M, Richards N, Davey GI, Levine E, Kelleher JH, Agley CC, Denk F, Harridge SD, McMahon SB. Defining the nociceptor transcriptome. Frontiers in molecular neuroscience. 2014; 7:87. [PubMed: 25426020]

67. Thompson JC, Dunbar E, Laye RR. Treatment challenges and complications with ziconotide monotherapy in established pump patients. Pain physician. 2006; 9(2):147–152. [PubMed: 16703976]

68. Tran-Van-Minh A, Dolphin AC. The alpha2delta ligand gabapentin inhibits the Rab11-dependent recycling of the calcium channel subunit alpha2delta-2. The Journal of neuroscience : the official journal of the Society for Neuroscience. 2010; 30(38):12856–12867. [PubMed: 20861389]

69. Wallace MS, Charapata SG, Fisher R, Byas-Smith M, Staats PS, Mayo M, McGuire D, Ellis D. Intrathecal ziconotide in the treatment of chronic nonmalignant pain: a randomized, double-blind, placebo-controlled clinical trial. Neuromodulation : journal of the International Neuromodulation Society. 2006; 9(2):75–86. [PubMed: 22151630]

70. Wang Y, Khanna R. Voltage-Gated Calcium Channels Are Not Affected by the Novel Anti-Epileptic Drug Lacosamide. Translational neuroscience. 2011; 2(1):13–22. [PubMed: 21949591]

71. Wang Y, Wilson SM, Brittain JM, Ripsch MS, Salome C, Park KD, White FA, Khanna R, Kohn H. Merging Structural Motifs of Functionalized Amino Acids and alpha-Aminoamides Results in Novel Anticonvulsant Compounds with Significant Effects on Slow and Fast Inactivation of Voltage-gated Sodium Channels and in the Treatment of Neuropathic Pain. ACS chemical neuroscience. 2011; 2(6):317–322. [PubMed: 21765969]

72. Webster LR, Fisher R, Charapata S, Wallace MS. Long-term intrathecal ziconotide for chronic pain: an open-label study. Journal of pain and symptom management. 2009; 37(3):363–372. [PubMed: 18715748]

73. Wei H, Karimaa M, Korjamo T, Koivisto A, Pertovaara A. Transient receptor potential ankyrin 1 ion channel contributes to guarding pain and mechanical hypersensitivity in a rat model of postoperative pain. Anesthesiology. 2012; 117(1):137–148. [PubMed: 22588108]

74. Wen H, Linhoff MW, Hubbard JM, Nelson NR, Stensland D, Dallman J, Mandel G, Brehm P. Zebrafish calls for reinterpretation for the roles of P/Q calcium channels in neuromuscular transmission. The Journal of neuroscience : the official journal of the Society for Neuroscience. 2013; 33(17):7384–7392. [PubMed: 23616544]

75. Wheeler DG, Groth RD, Ma H, Barrett CF, Owen SF, Safa P, Tsien RW. Ca(V)1 and Ca(V)2 channels engage distinct modes of Ca(2+) signaling to control CREB-dependent gene expression. Cell. 2012; 149(5):1112–1124. [PubMed: 22632974]

76. Wilson SM, Brittain JM, Piekarz AD, Ballard CJ, Ripsch MS, Cummins TR, Hurley JH, Khanna M, Hammes NM, Samuels BC, White FA, Khanna R. Further insights into the antinociceptive potential of a peptide disrupting the N-type calcium channel-CRMP-2 signaling complex. Channels (Austin). 2011; 5(5):449–456. [PubMed: 21829088]

77. Wilson SM, Khanna R. Specific binding of lacosamide to collapsin response mediator protein 2 (CRMP2) and direct impairment of its canonical function: implications for the therapeutic potential of lacosamide. Molecular neurobiology. 2015; 51(2):599–609. [PubMed: 24944082]

78. Wilson SM, Moutal A, Melemedjian OK, Wang Y, Ju W, Francois-Moutal L, Khanna M, Khanna R. The functionalized amino acid (S)-Lacosamide subverts CRMP2-mediated tubulin

polymerization to prevent constitutive and activity-dependent increase in neurite outgrowth. Frontiers in cellular neuroscience. 2014; 8:196. [PubMed: 25104922]

79. Wilson SM, Schmutzler BS, Brittain JM, Dustrude ET, Ripsch MS, Pellman JJ, Yeum TS, Hurley JH, Hingtgen CM, White FA, Khanna R. Inhibition of transmitter release and attenuation of anti-retroviral-associated and tibial nerve injury-related painful peripheral neuropathy by novel synthetic Ca2+ channel peptides. The Journal of biological chemistry. 2012; 287(42):35065–35077. [PubMed: 22891239]
80. Yaksh TL, Rudy TA. Chronic catheterization of the spinal subarachnoid space. Physiology & behavior. 1976; 17(6):1031–1036. [PubMed: 14677603]
81. Yamamoto S, Ohsawa M, Ono H. Contribution of TRPV1 receptor-expressing fibers to spinal ventral root after-discharges and mechanical hyperalgesia in a spared nerve injury (SNI) rat model. J Pharmacol Sci. 2013; 121(1):9–16. [PubMed: 23238537]
82. Yamashita N, Ohshima T, Nakamura F, Kolattukudy P, Honnorat J, Mikoshiba K, Goshima Y. Phosphorylation of CRMP2 (collapsin response mediator protein 2) is involved in proper dendritic field organization. The Journal of neuroscience : the official journal of the Society for Neuroscience. 2012; 32(4):1360–1365. [PubMed: 22279220]
83. Yang YR, He Y, Zhang Y, Li Y, Li Y, Han Y, Zhu H, Wang Y. Activation of cyclin-dependent kinase 5 (Cdk5) in primary sensory and dorsal horn neurons by peripheral inflammation contributes to heat hyperalgesia. Pain. 2007; 127(1–2):109–120. [PubMed: 16996690]
84. Zamponi GW, Lewis RJ, Todorovic SM, Arneric SP, Snutch TP. Role of voltage-gated calcium channels in ascending pain pathways. Brain research reviews. 2009; 60(1):84–89. [PubMed: 19162069]
85. Zhou Y, Cattley RT, Cario CL, Bai Q, Burton EA. Quantification of larval zebrafish motor function in multiwell plates using open-source MATLAB applications. Nat Protoc. 2014; 9(7):1533–1548. [PubMed: 24901738]

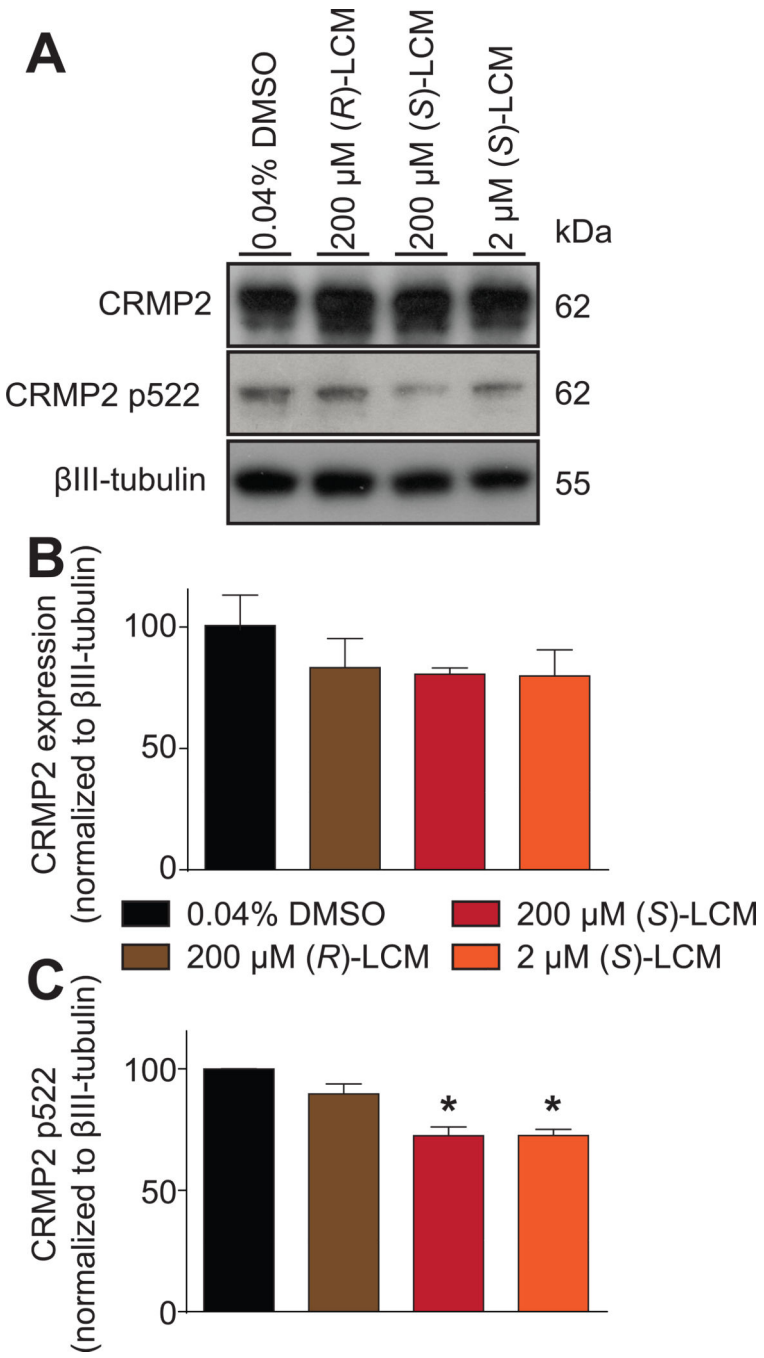

Figure 1. (*S*)-LCM inhibits CRMP2 phosphorylation in sensory neurons

(**A**) Representative Western blots of lysates prepared from DRGs incubated for 30 min with vehicle (0.04% DMSO), (*R*)-LCM (200 µM) or (*S*)-LCM (200 µM or 2µM), probed with the indicated CRMP2 and phospho-specific CRMP2 antibodies. The positions of molecular weight markers (kilodaltons, kD) are illustrated on the right. βIII-tubulin is used as a loading control. (**B**) Summary of the mean relative levels of CRMP2 (normalized to βIII-tubulin) in arbitrary units (a.u.). Neither treatment significantly affected CRMP2 expression ($n = 3$ wells per condition). (**C**) Summary of the mean relative levels of phospho-CRMP2 (p522)

(normalized to CRMP2 levels and βIII-tubulin) in arbitrary units (a.u.). (*S*)-LCM treatments significantly decreased CRMP2 phosphorylation levels while (*R*)-LCM had no effect ($n = 3$ wells per condition). Asterisks indicate statistical significance compared with control cells ($p<0.05$, Kruskal–Wallis non-parametric test with a Dunnett's *post hoc* analysis).

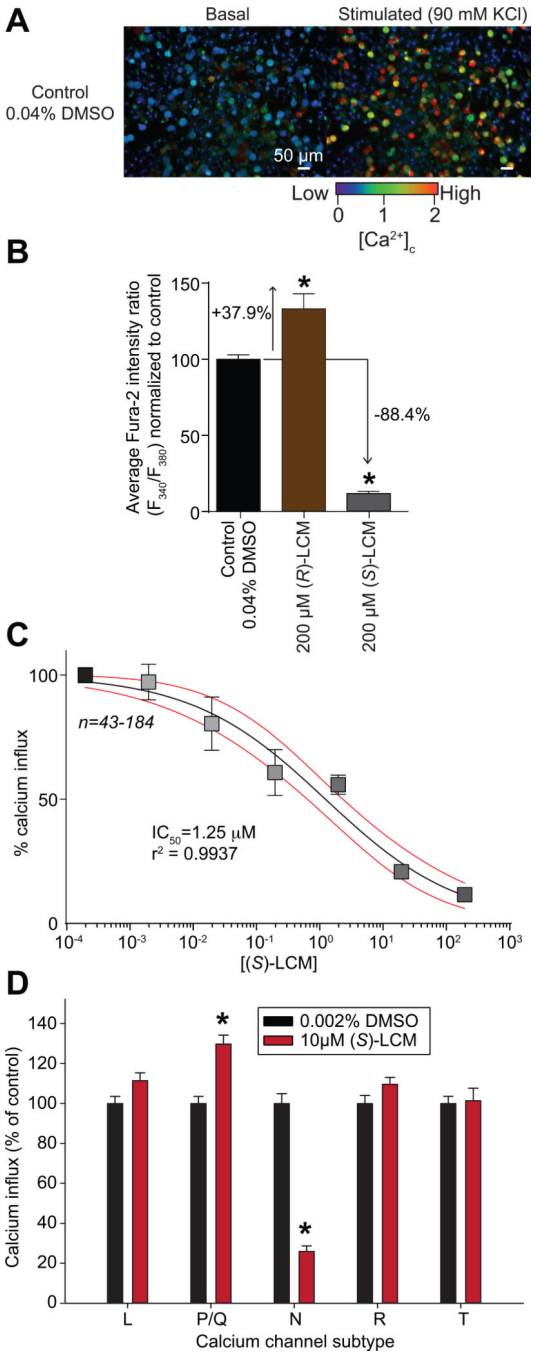

Figure 2. Concentration-dependent inhibition of (*S*)-LCM on depolarization-evoked Ca^{2+} influx in dorsal root ganglion (DRG) neurons

(**A**) Pseudocolored fluorescent images of a field of DRG neurons visualized for Fura-2AM, before (basal) and after (stimulated) a challenge with 90 mM KCl for control (DMSO-treated) neurons. Following a 1-min baseline measurement, neurons were stimulated with 90mM KCl for 15 s and the response measured for 3 additional minutes. Scale bar is 50 µm. Fluorescent scale shows the relative intracellular calcium concentration $[Ca^{2+}]_c$ in each neuron. (**B**) Bar graphs show the normalized peak fluorescence response (adjusted for

background) of DRGs incubated for 30 min with vehicle (0.04% DMSO) or 200 μM of either (*R*)-LCM or (*S*)-LCM. Values represent the average ± S.E.M., n=94-205 cells per condition. Asterisks indicate statistical significance compared with control cells ($p<0.05$, 1-way analysis of variance with Dunnett's post hoc analysis). (**C**) Concentration-dependent effect of *S*)-LCM on depolarization-evoked Ca^{2+} influx in sensory neurons. Percent inhibition of peak Ca^{2+} influx normalized to the control is plotted for various concentrations of (*S*)-LCM. The data were fitted in GrpahPad Prism with a log(inhibitor) versus normalized response with variable slope curve which yielded an IC_{50}=1.25 μM with r^2=0.9937. (**D**) Bar graphs show the normalized peak fluorescence response (normalized to vehicle) of DRGs incubated for 30 min with vehicle (0.002% DMSO) or 10 μM (*S*)-LCM in the presence of pharmacological blockers (see Methods for details) specific for the indicated calcium channel subtypes. Values represent the average ± S.E.M., n=93-349 cells per condition. Asterisks indicate statistical significance compared with control cells ($p<0.05$, Student's t-test).

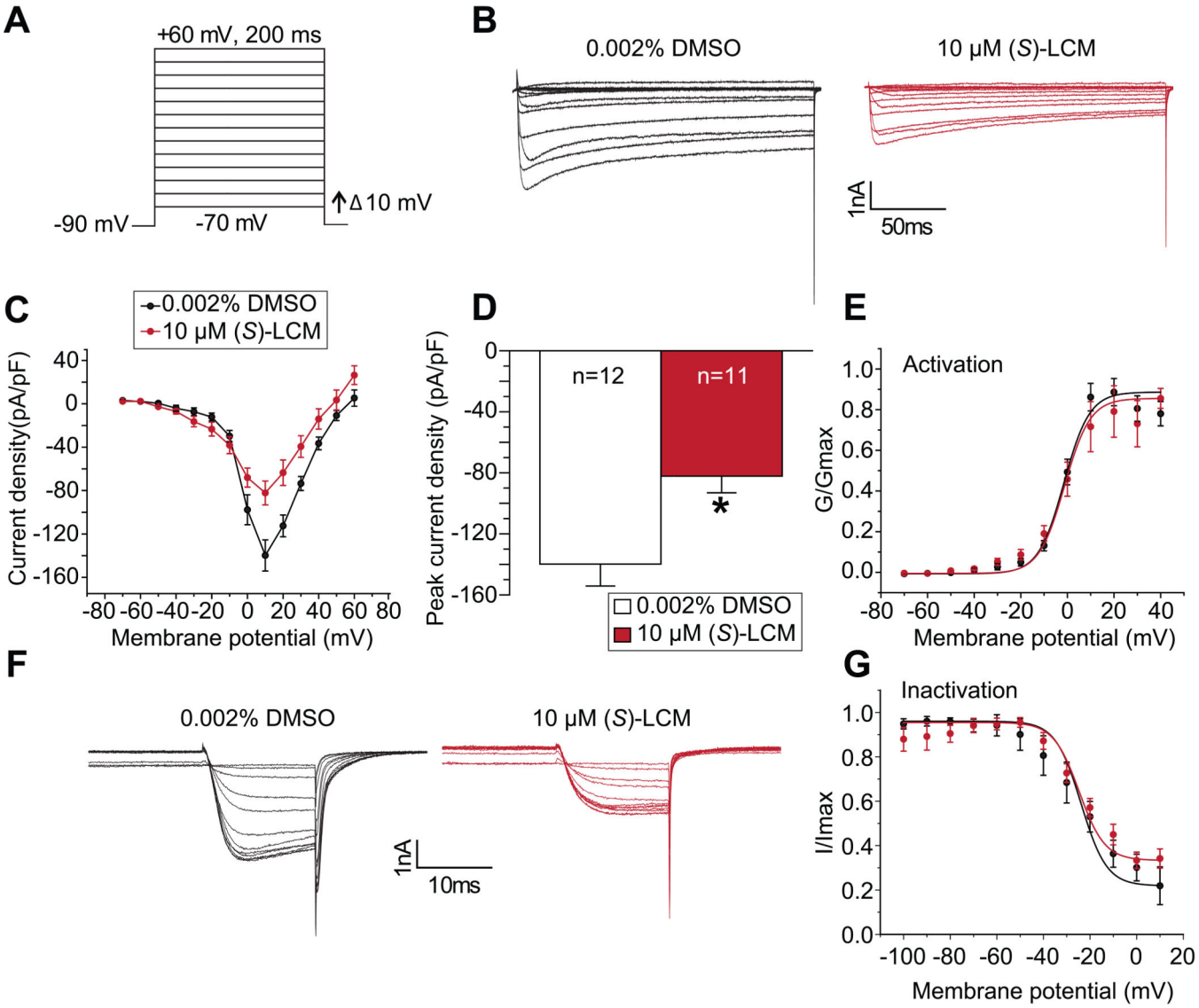

Figure 3. Acute application of (*S*)-LCM decreases Ca^{2+} currents in sensory neurons

(**A**) Voltage protocol used to evoke Ca^{2+} currents. Currents were evoked by 200 millisecond prepulses between −90 mV and +60 mV. (**B**) Representative family of current traces are illustrated for control- (0.002% DMSO) or 10 μM (*S*)-LCM-treated. (**C**) Summary of the current density (pA/pF) versus membrane potential curves from sensory neurons in the absence or presence of 10 μM (*S*)-LCM. (**D**) Peak current density, at −10 mV, for the indicated conditions (n=12 cells for control and n=11 cells for 10 μM (*S*)-LCM treated cells; asterisk indicates statistical significance compared with control cells ($p<0.05$, Student's t-test). (**E**) Boltzmann fits for activation for DRGs treated as indicated. Values for $V_{1/2}$, the voltage of half-activation, and slope factors (*k*) were not different between the two conditions. (**F**) Representative family of current traces for Ca^{2+} channel inactivation are illustrated for control- (0.002% DMSO) or 10 μM (*S*)-LCM-treated (n=6 cells per condition). Currents were elicited in response to pre-conditioning pulse of –100mV to 10mV, in 10mV increments, for 1.5s duration followed by a depolarizing test pulse to 10mV

for 20ms. (**G**) Boltzmann fits for channel inactivation for DRGs treated as indicated. Values for $V_{1/2}$, the voltage of half-inactivation, and slope factors (*k*) were not different between the two conditions.

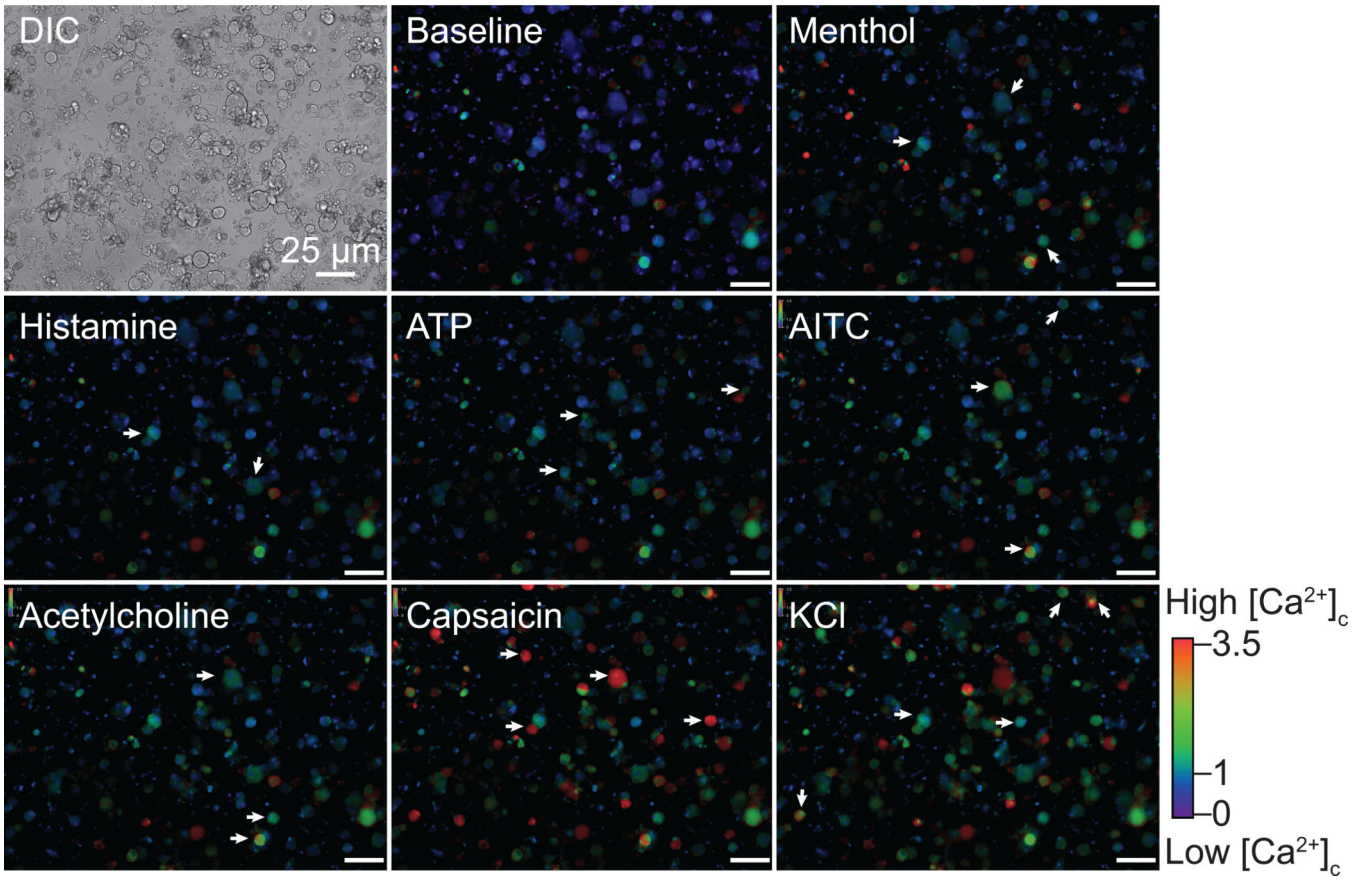

Figure 4. DRG neuronal responses to constellation pharmacology triggers

Differential interference contrast (DIC) and pseudocolored fluorescent images of the same field of view. The baseline shows the fluorescence ratio per cell before the constellation pharmacology protocol. Each constellation pharmacology trigger was applied for 15 s. Pseudocolored images show the cytoplasmic Ca^{2+} concentration after the application of each trigger on the DRG neurons. Arrows show examples of cells responding to the indicated trigger. The colored scale indicates the value of the Fura-2AM fluorescence ratio (F_{340}/F_{380}). High values correspond to high intracellular Ca^{2+} concentration (red). Scale bar is 25 μm. Images are from control DRG neurons treated with vehicle (0.002% DMSO).

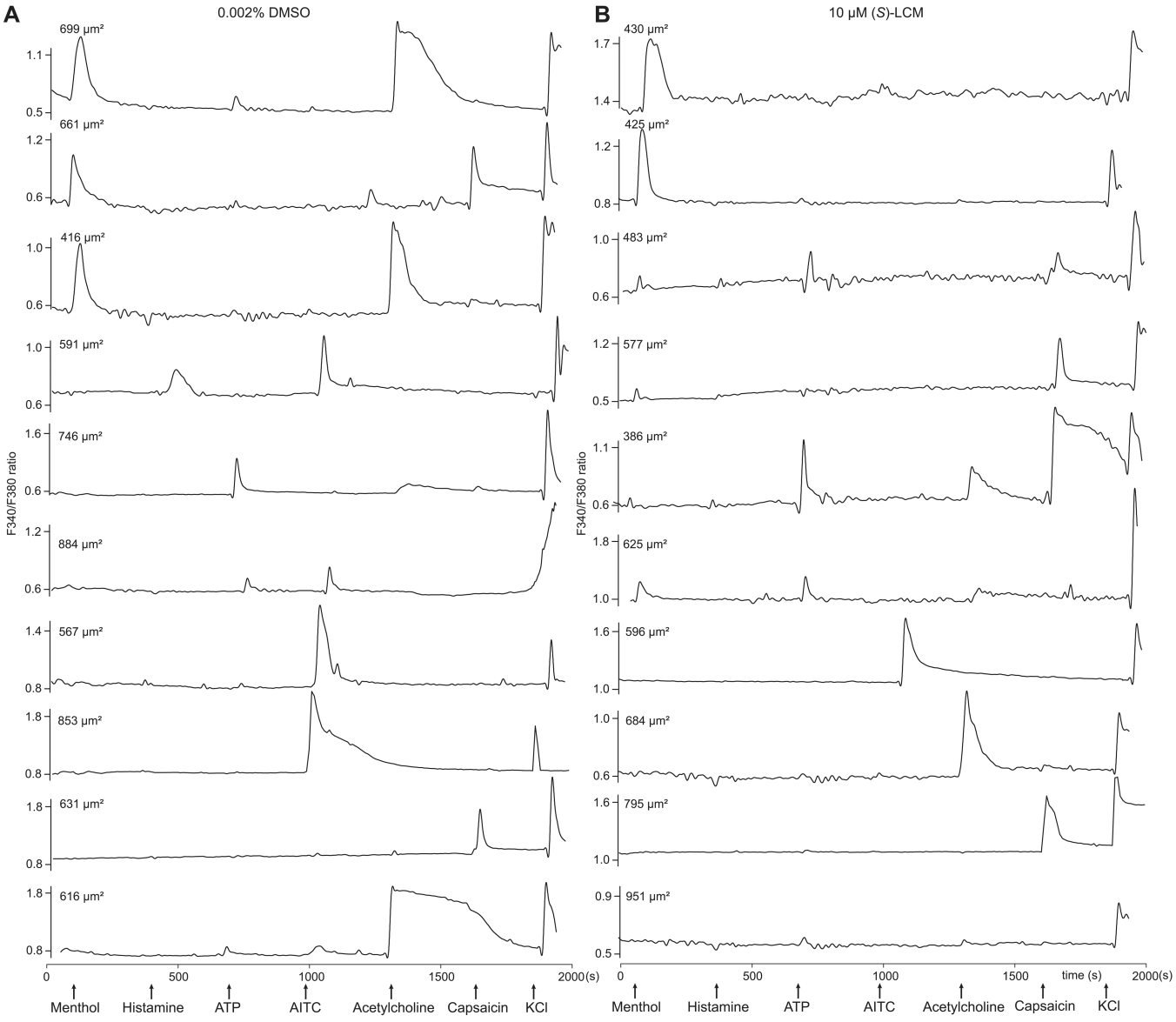

Figure 5. Ca^{2+}-imaging traces of DRGs responding to constellation pharmacology agonist or membrane-potential triggers

Each trace represents the response of a different neuron. In a typical experimental trial, the responses of >100 individual neurons were monitored simultaneously. Selected traces are shown. The abbreviations used are defined in Table 1. Arrows indicate the ~15-s application of challenge compounds or high [K+]o; after each application the free compound or high [K+]o was continuously washed out of the well with room-temperature bath solution. The y-axis shows the Fura-2AM fluorescence ratio (F_{340}/F_{380}) for each trace. Raw, unfiltered traces are presented. Triggers used were: menthol (400 nM), histamine (50 μM), ATP (10 μM), AITC (200 μM), acetylcholine (1 mM), capsaicin (100 nM) and KCl (90 mM). DRG neurons were treated with either vehicle (0.002% DMSO) (**A**) or 10 μM (S)-LCM (**B**) and the neuronal populations analyzed by the constellation pharmacology protocol. All cells

were selected based on their response to the depolarizing pulse of KCl. Size of each cell is indicated by the surface area value in each trace.

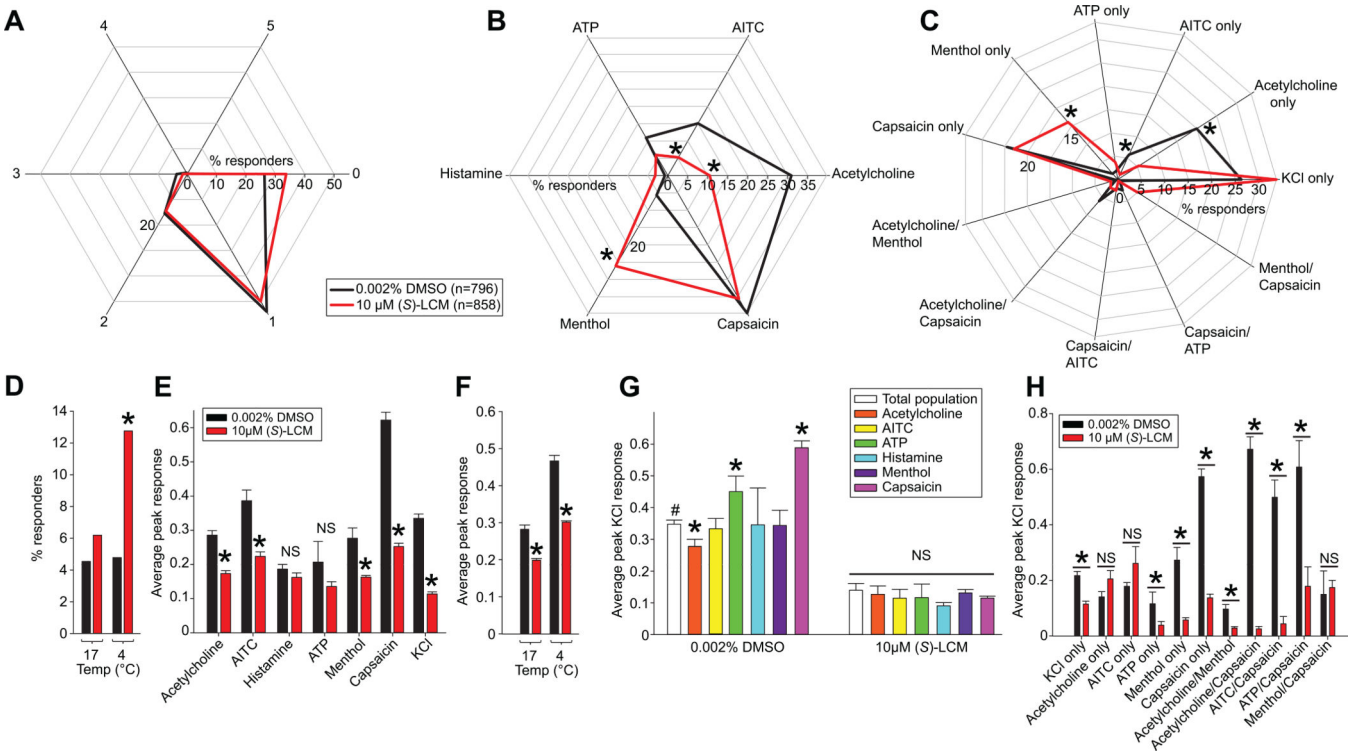

Figure 6. Functional 'fingerprinting' of DRG neuronal subclasses following treatment with (*S*)-LCM

(**A**) The response of DRG neurons to one or more constellation pharmacology trigger was analyzed. The polar plot indicates the percentage of cells that responded to the indicated number of triggers independently of which compound they responded to. The number 0 corresponds to the proportion of cells that responded to KCl only and no other trigger. No significant change was observed in each category of cells after treatment with (*S*)-LCM. (**B**) Polar plot showing the percent of cells responding to each constellation pharmacology trigger independently of any other trigger that the cell also responded to. Each axis shows a different trigger. (*S*)-LCM significantly decreased the percent of cells responding to acetylcholine and AITC, but decreased the percent of cells responding to menthol (*S*)-LCM (z-test). (**C**) The major neuronal classes identified in both conditions. The functional neuronal population responding to menthol only and both menthol and capsaicin were enriched in (*S*)-LCM-treated DRG neurons. There was a decrease in the functional neuronal populations responding to AITC only, acetylcholine only and acetylcholine/capsaicin with (*S*)-LCM treatment. Asterisks indicates statistical significance ($p<0.05$, z-test), data from 4 independent experiments with a total n=796 for control and n=856 for 10μM (*S*)-LCM. (**D**) Bar graph showing the percentage of cell responding to cold temperature (17°C or 4°C) stimuli. (*S*)-LCM significantly increased the percent of cells responding to 4°C. Asterisks indicates statistical significance (*, $p<0.05$, z-test; n=368 for control and n=398 for 10 μM (*S*)-LCM). (**E**) Bar graph showing the average peak response elicited by each constellation pharmacology trigger in DRG neurons treated with vehicle or 10 μM (*S*)-LCM. Significant decreases in average peak response for acetylcholine, AITC, Menthol and Capsaicin were observed. The decrease observed in KCl peak shows the efficiency of the (*S*)-LCM

treatment corroborating results in earlier experiments (see Fig. 3) (*, $p<0.05$; Student's t-test). (**F**) Bar graph showing the average peak response elicited by each cold temperature in DRG neurons treated with vehicle (n=368) or 10 μM (*S*)-LCM (n=398). Significant decreases in average peak response for both temperatures were observed (*, $p<0.05$; Student's t-test). (**G**) Bar graph showing the average peak KCl response in different functional neuronal populations after vehicle or (*S*)-LCM treatment. The control condition shows different KCl peak responses between neuronal populations in the control condition while the (S)-LCM treatment inhibited Ca^{2+} influx in all functional populations. (*, $p<0.05$; one way ANOVA). (**H**) Bar graph showing the average peak KCl response in the major functional neuronal populations identified in (**C**). (S)-LCM did not decrease the KCl response in Acetylcholine only and menthol/capsaicin responding cell populations (*, $p<0.05$; Student's t-test).

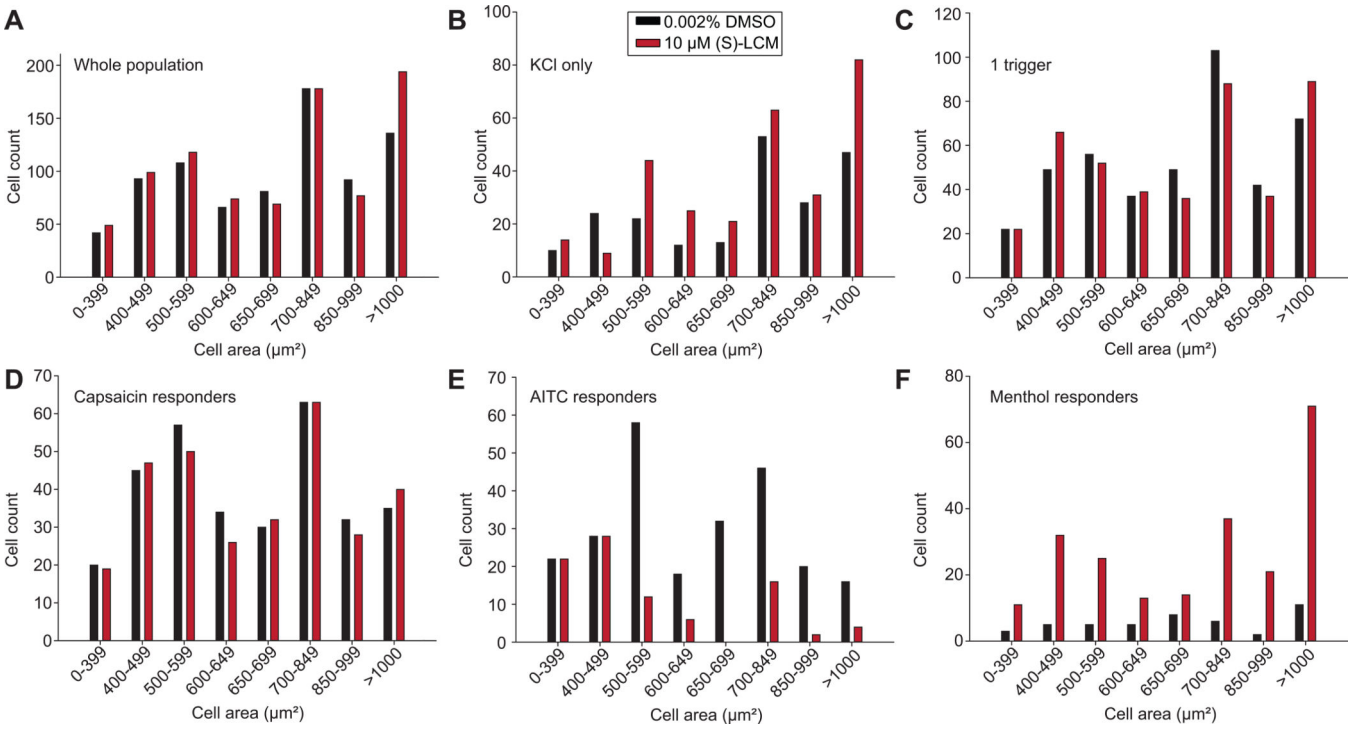

Figure 7. Size distribution of neurons responsive to specific constellation pharmacology triggers

Data for select neuronal classes is shown. For all panels, the x-axis represents the cell area (classified according to the indicated intervals) and the y-axis denotes the number of cells corresponding to the indicated trigger combination for each condition (0.002% DMSO or 10 μM (*S*)-LCM). Bar graphs of sizes of neurons representing the entire population (**A**), KCl responders (**B**), KCl plus one other trigger responders (**C**), capsaicin responders (**D**), AITC responders, (**E**) or Menthol responders (**F**).

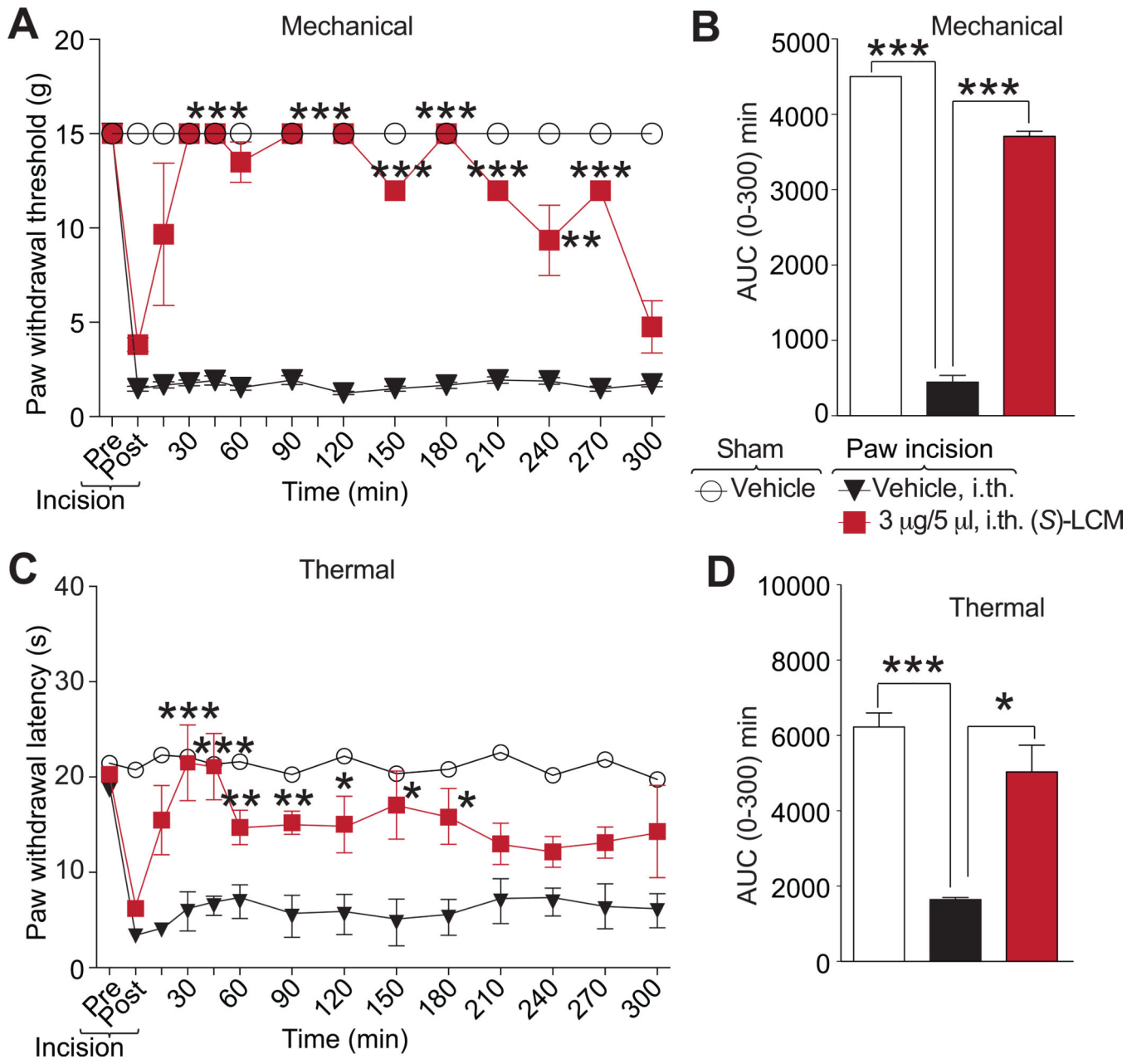

Figure 8. (*S*)-LCM decreases plantar incision-induced thermal hyperalgesia and mechanical allodynia

Rats received a plantar incision on the left hind paw. Paw withdrawal latencies (PWLs) were significantly decreased 24 hours after incision. (*S*)-LCM (3 μg/5 mL) or vehicle (saline) were injected into the intrathecal space and PWLs measured. Paw withdrawal latencies were significantly reversed at the indicated times after injection of (*S*)-LCM (**A**) (n=12 for vehicle and n=9 for (*S*)-LCM; **p<0.05; and ***p<0.001; Student's t-test). Likewise, paw withdrawal thresholds (PWTs) were significantly decreased 24 hours after incision. Injection of (*S*)-LCM (**C**) significantly reversed PWTs at the indicated times (n=4; *p<0.05; and ***p<0.001; Student's t-test). Area under the curve (AUC), using the trapezoid method, for

PWL (**B**; summary for data shown in **A**) and PWT (**D**; summary for data shown in **C**) are shown.

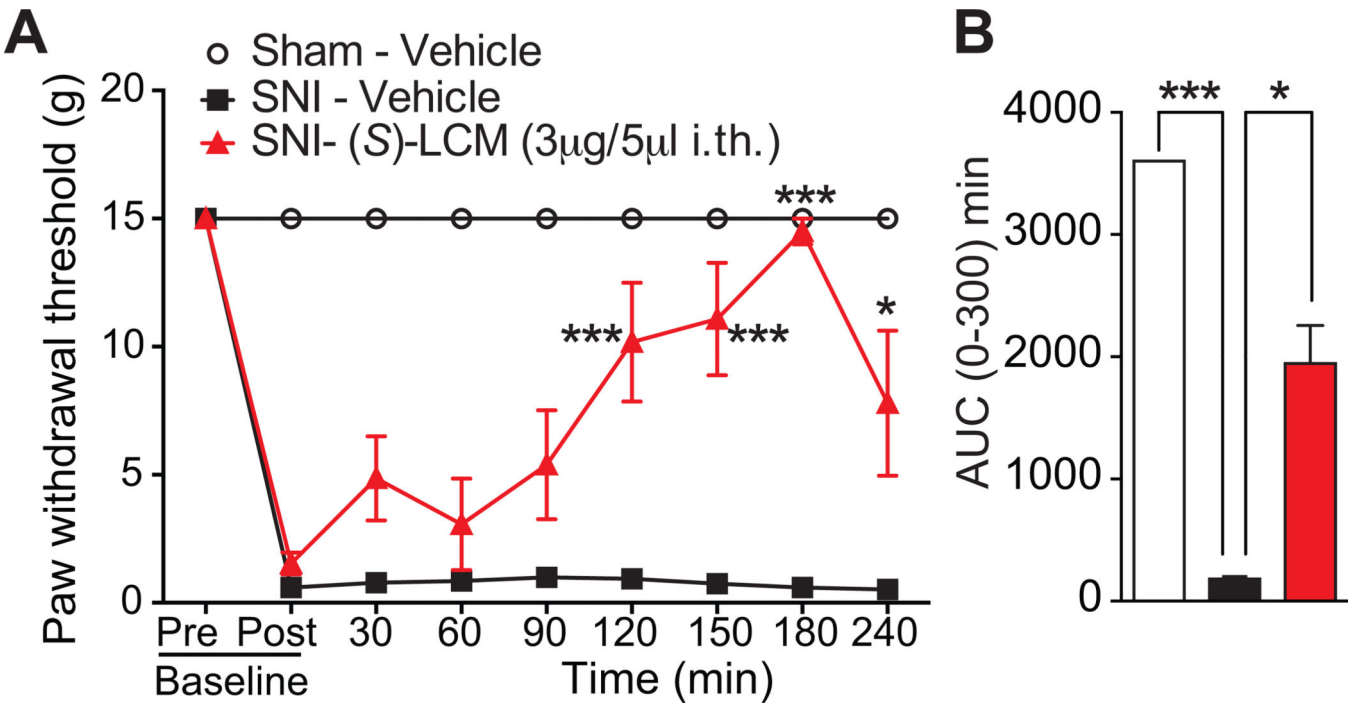

Figure 9. (*S*)-LCM decreases mechanical allodynia after neuropathic injury

Rats received spared nerve injury on the left hind paw. Paw withdrawal thresholds (PWTs) were significantly decreased 24 hours after incision. (*S*)-LCM (3 μg/5 mL) or vehicle (saline) were injected into the intrathecal space and PWTs measured. Paw withdrawal thresholds were significantly reversed at the indicated times after injection of (*S*)-LCM (**A**) (n=6; *p<0.05; and ***p<0.001; Student's t-test). Area under the curve (AUC), using the trapezoid method, for PWT (**B**; summary for data shown in **A**) is shown.

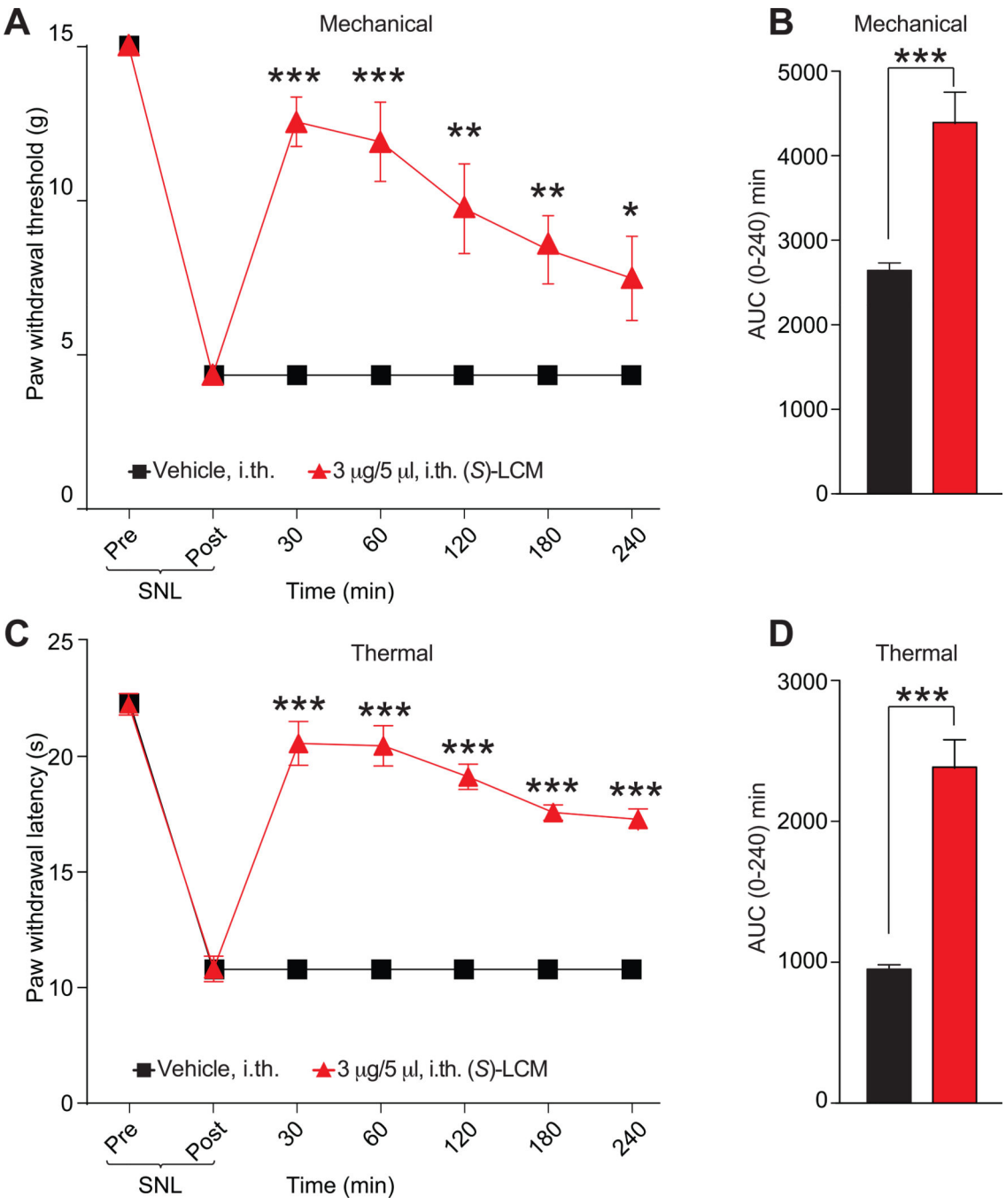

Figure 10. (*S*)-LCM decreases thermal hyperalgesia and mechanical allodynia after spinal nerve ligation

Rats received spinal nerve ligation (SNL) injury on the left hind paw. Paw withdrawal thresholds (PWTs) were significantly decreased 7 days after surgery. (*S*)-LCM (3 μg/5 μL) or vehicle (saline) were injected into the intrathecal space and PWTs measured. Paw withdrawal thresholds were significantly reversed at the indicated times after injection of (*S*)-LCM (**A**) (n=6; *p<0.05; and ***p<0.001; two-way ANOVA). Likewise, paw withdrawal thresholds (PWTs) were significantly decreased for 4 hours. Injection of (*S*)-

LCM (**C**) significantly reversed PWTs at the indicated times (n=6; ***p<0.0001; Two-way ANOVA). Area under the curve (AUC), using the trapezoid method, for PWL (**B**; summary for data shown in **A**) and PWT (**D**; summary for data shown in **C**) are shown.

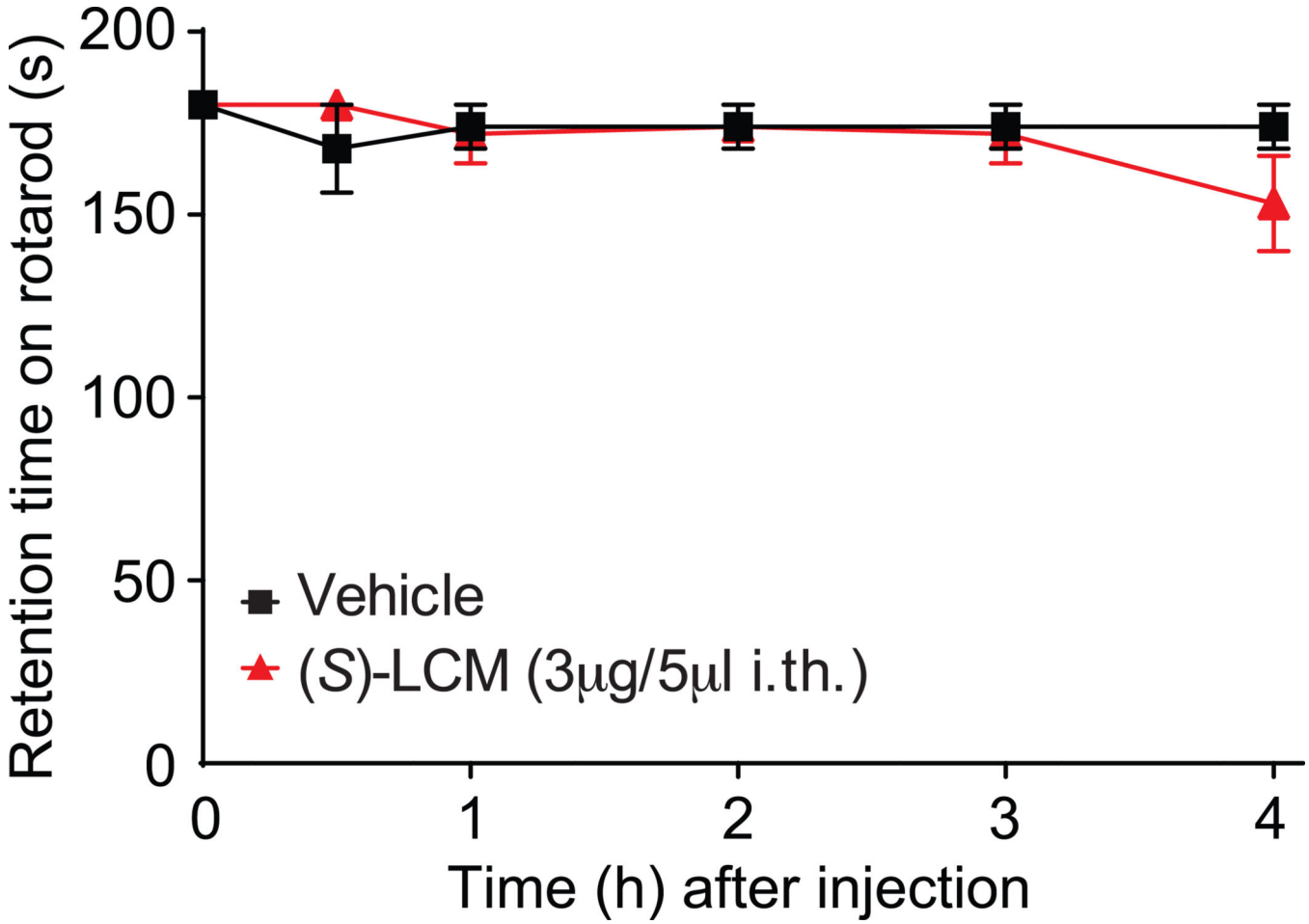

Figure 11. Spinal administration of (*S*)-LCM did not result in motor deficits or sedation

(*S*)-LCM (3 µg/5 µL i.th.) or vehicle (0.9 % saline) was evaluated for motor deficits using the rotarod performance test. Vehicle-treated animals and (*S*)-LCM –treated animals remained on the rotarod for 180 seconds at each time point over the course of 240 minutes. Animals treated with (*S*)-LCM remained on the rotarod for an average of 178 seconds, a value that was not significantly different from vehicle treated animals and baseline values. N=6 rats per condition.

Table 1

Percent of DRG neurons responding to constellation pharmacology triggers.

		0.002% DMSO		10 μM (*S*)-LCM	
Compound	**Final concentration**	**Number of cells**	**% of total**	**Number of cells**	**% of total**
Menthol	400 μM	45	5.7	224	26.1
Histamine	50 μM	6	0.8	27	3.2
ATP	10 μM	87	11.0	51	5.9
AITC	200 μM	120	15.1	45	5.3
Acetylcholine	1 mM	246	30.9	90	10.5
Capsaicin	100 nM	316	39.7	305	35.6
KCl	90 mM	796	100.0	858	100.0

The numbers are from four separate experiments for each treatment condition. Abbreviations: ATP, adenosine triphosphate; AITC, Allyl Isothiocyanate (mustard oil); KCl, potassium chloride.